TAp73 is essential for germ cell adhesion and maturation in testis

Lena Holembowski,[1] Daniela Kramer,[1] Dietmar Riedel,[3] Raffaella Sordella,[4] Alice Nemajerova,[2] Matthias Dobbelstein,[1] and Ute M. Moll[1,2]

[1]Department of Molecular Oncology, University of Göttingen, 37077 Göttingen, Germany
[2]Department of Pathology, Stony Brook University, Stony Brook, NY 11794
[3]Max Planck Institute for Biophysical Chemistry, 37077 Göttingen, Germany
[4]Cold Spring Harbor Laboratory, Cold Spring Harbor, NY 11724

A core evolutionary function of the p53 family is to protect the genomic integrity of gametes. However, the role of p73 in the male germ line is unknown. Here, we reveal that TAp73 unexpectedly functions as an adhesion and maturation factor of the seminiferous epithelium orchestrating spermiogenesis. TAp73 knockout (TAp73KO) and p73KO mice, but not ∆Np73KO mice, display a "near-empty seminiferous tubule" phenotype due to massive premature loss of immature germ cells. The cellular basis of this phenotype is defective cell–cell adhesions of developing germ cells to Sertoli nurse cells, with likely secondary degeneration of Sertoli cells, including the blood–testis barrier, which leads to disruption of the adhesive integrity and maturation of the germ epithelium. At the molecular level, TAp73, which is produced in germ cells, controls a coordinated transcriptional program of adhesion- and migration-related proteins including peptidase inhibitors, proteases, receptors, and integrins required for germ–Sertoli cell adhesion and dynamic junctional restructuring. Thus, we propose the testis as a unique organ with strict division of labor among all family members: p63 and p53 safeguard germ line fidelity, whereas TAp73 ensures fertility by enabling sperm maturation.

Introduction

The process of producing high-quality, fertile sperm requires many steps. It takes place in the germ epithelium of testis, which consists of highly ordered layers of developing germ cells lining the seminiferous tubules. Mice reach fertility at 6–7 wk of age, after which spermatozoa are continuously produced (Borg et al., 2010). Diploid stem cells at the basement membrane (BM) ensure permanent production of spermatogonia, which develop into mature sperm during "seminiferous cycles." Spermatogonia first enter meiosis to produce haploid spermatocytes. Subsequently, spermatocytes enter spermiogenesis, where they undergo major morphological changes that ultimately result in the formation of an acrosome and a flagellum, with condensation of the nucleus and elimination of the cytoplasm. Mature motile elongated spermatids are then released into the lumen by spermiation and travel to the downstream epididymis, where they undergo further minor maturation and final storage in the caudal part until ejaculation (Cooke and Saunders, 2002; Fig. S1 A).

Sperm production in the seminiferous epithelium critically depends on interspersed Sertoli cells. These tall somatic cells stretch from the BM through the entire epithelium into the lumen, with each Sertoli cell enveloping 30–50 developing germ cells in deep cytoplasmic pockets. They exert a crucial nursing role, providing physical support, transport, nutrients, and paracrine signals for the nascent sperm (Griswold, 1998). Thus, during their differentiation, germ cells migrate upwards into the apical lumen within nursing pockets, while constantly detaching and reattaching from the Sertoli cells via dynamic cell–cell junctional restructuring (Mruk and Cheng, 2004). During that journey they also pass the blood–testis barrier (BTB), which consists of tight-, gap-, adherens-, and desmosome-like junctions between Sertoli–Sertoli

The Rockefeller University Press $30.00
J. Cell Biol. Vol. 204 No. 7   1173–1190
www.jcb.org/cgi/doi/10.1083/jcb.201306066

JCB   1173

cells that physically separate the basal stem cell niche from the apical differentiation compartment. Thus, the BTB protects developing germ cells, which express a unique protein profile within the body, from autoimmune reactions and exogenous toxins (Xia et al., 2005). Failure at various steps of spermatogenesis or structural defects of the seminiferous epithelium can lead to infertility and/or genetically unstable sperm.

The p53 homologues p63 and p73 are emerging as crucial guardians of the germ line in development and adult life, safeguarding against DNA damage by eliminating genetically unstable cells via apoptosis. Like p53, p63 and p73 are transcription factors with high homology in the transactivation (TA), DNA-binding, and oligomerization domains. Like p63, p73 has two isoforms that either harbor an N-terminal TA domain (TAp73) or lack it (ΔNp73). ΔNp73 is a dominant-negative inhibitor of TAp73/TAp63/p53 functions, mostly via mixed oligomerization (Dötsch et al., 2010). A common p63/p73-like ancestor exists in the modern-day sea anemone *Nematostella vectensis*, where nvp63 acts as protector against DNA damage in gametes, driving their apoptosis and thereby ensuring genetic stability and production of healthy offspring (Pankow and Bamberger, 2007). In mammals, TAp63, but not p53, is the main guardian of the female germ line. Upon γ irradiation, TAp63-specific knockout (KO) mice fail to remove damaged, genetically unstable oocytes, whereas wild-type (WT) and p53-null mice reduce the primordial follicle pool by 90% (Suh et al., 2006). Likewise, in the male germ line in hominids, a unique isoform called GTAp63 induces apoptosis in response to genotoxic stress. GTAp63, driven by the long terminal repeat promoter of an upstream endogenous retrovirus (ERV9), is highly expressed in germ cell precursors in human testis as the sole p63 species (Beyer et al., 2011).

In the female germ line, TAp73 also protects genomic integrity and fertility. Female TAp73KO mice are infertile due to poor oocyte quality, with increased spindle abnormalities causing multinucleated blastomeres, and defects in the ovulation release of the egg. Notably, male TAp73KO mice were also reported as infertile but not studied further (Tomasini et al., 2008). Thus, in contrast to the clear pro-death function of p53 and p63 in response to germ cell damage, the exact role of p73 in the male germ line (i.e., why p73 is critical) is currently unknown. Here, we uncover an unexpected function of TAp73 as an adhesive homeostatic factor, which is indispensable to orchestrate normal maturation and adhesion of germ cells within the adult seminiferous epithelium by regulating their interaction with Sertoli cells, thereby ensuring male fertility.

Results

Loss of TAp73 leads to depletion of developing and mature germ cells from the seminiferous epithelium

TAp73-specific and global p73KO mice are essentially infertile for both sexes (Tomasini et al., 2008; Yang et al., 2000). Female infertility in TAp73KO mice is caused by genomic instability of oocytes paired with ovulation defects (Tomasini et al., 2008), which are likely enhanced by abnormal mating behavior due to defects in the vomeronasal organ (Yang et al., 2000). However,

male infertility in TAp73KO mice (some being only subfertile rather than completely sterile; Fig. S1 B) remains unexplained. To identify its cause, we compared testis histology of global and isoform-specific KO with WT littermate mice at different ages. The developing testis of immature mice (postnatal day 20 [P20]) showed no difference in hematoxylin and eosin (H&E) morphology (Fig. 1 A). Also, the anatomical size and weight of adult p73KO testis (P42) was normal (Fig. 1 B and Fig. S1 C). However, histologically adult p73KO testis revealed a striking phenotype of severe loss of developing germ cells and mature spermatozoa, creating "nearly empty" seminiferous tubules, compared with WT littermates (Fig. 1 B). An identical phenotype was observed in adult isoform-specific TAp73KO testes (P42; Fig. 1 C). Heterozygous (Het) p73 and TAp73 testes were identical to WT. In sharp contrast, loss of the transcriptionally inactive isoform ΔNp73 did not affect the seminiferous epithelium (Fig. 1 C and Fig. S1 D). In sum, p73/TAp73KO mice (*n* = 35) revealed a "germ-loss" phenotype mostly strong or medium in degree, with 100% penetrance, whereas ΔNp73KO testis never showed any morphological changes (Fig. 1 D). This is in accordance with TAp73 as the main isoform in WT testis, whereas ΔNp73 is barely detectable (Fig. 1 E). However, the hormonal hypothalamic–pituitary–testicular axis was not affected in p73KO and TAp73KO mice (Fig. S2). These data establish the finding that TAp73 is required for proper sperm maturation in the adult, whereas ΔNp73 is completely dispensable.
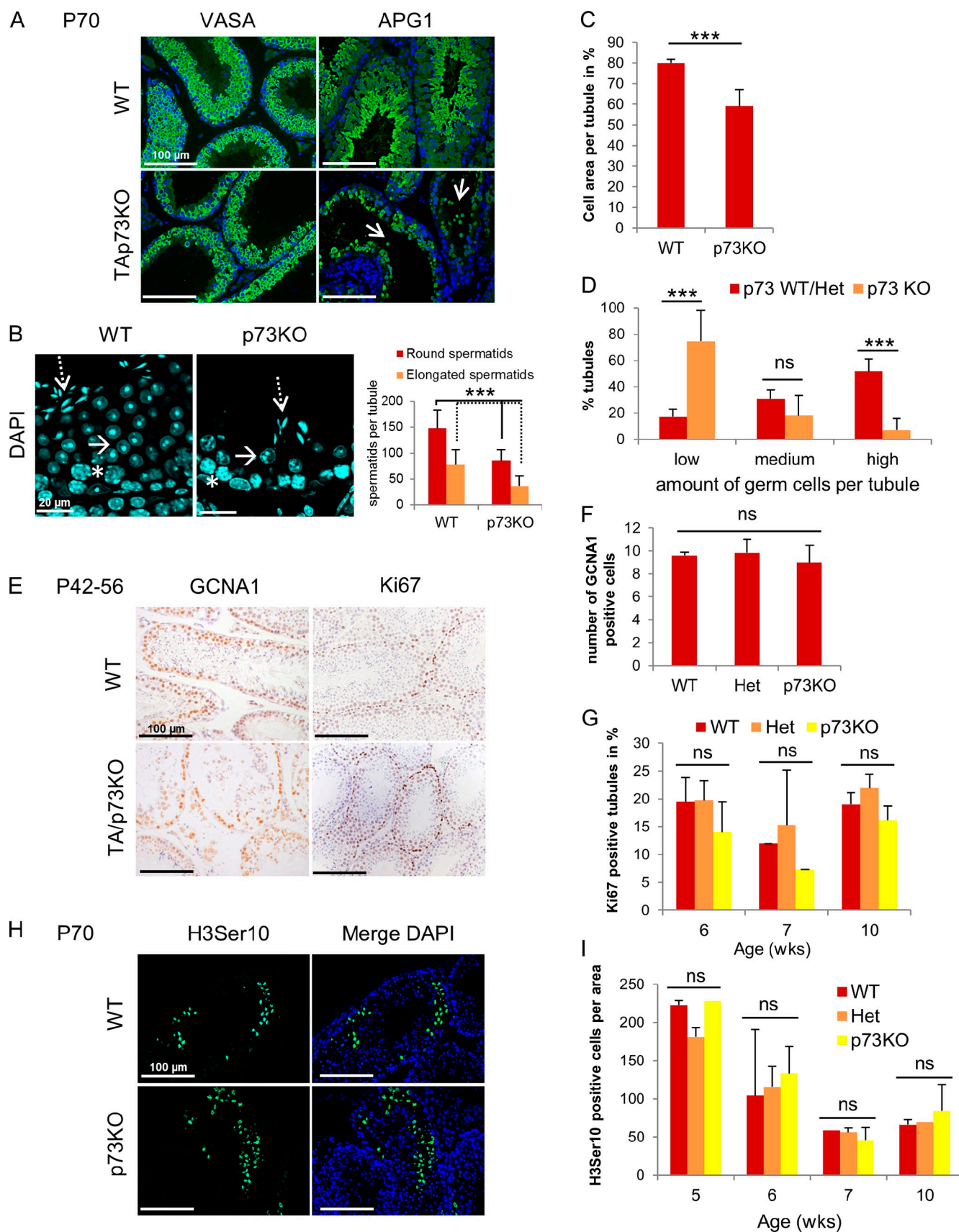
TAp73KO testis shows selective loss of round and elongated spermatids and spermatozoa

To identify which cell types are lost in KO seminiferous epithelium, we performed immunofluorescence (IF) analysis. Meiotic cells (spermatocytes) and round spermatids were identified by the VASA marker (aka DEAD box helicase protein DDX4 or MVH; Castrillon et al., 2000). Round and elongated spermatids and mature spermatozoa were identified by the specific APG1 marker (a member of the heat shock protein family HSP110; Held et al., 2006). Of note, TAp73KO seminiferous epithelium showed a mild-to-moderate reduction in (the more basal) VASA-positive cell layers and a strong reduction in apical layers, especially APG1-positive spermatids, compared with WT littermates (Fig. 2 A). Confocal microscopy of nuclear DAPI-stained sections confirmed that round and elongated spermatids are strongly reduced in the p73KO epithelium (Fig. 2 B, arrows). In contrast, pachytene spermatocytes were present in normal numbers (Fig. 2 B, left, asterisks). We quantified the tubules for degree of germ cell loss using H&E sections of p73KO versus WT and p73Het littermates (Fig. 2, C and D). p73KO mice display 20–30% loss in germ cell area per total tubular area (Fig. 2 C). Also, most p73KO tubules retained only a small number of germ cells, and tubules with a relatively high number of germ cells were rare (Fig. 2 D). Of note, this massive loss of maturing germ cells in upper cell layers was contrasted by a normal number of basal proliferating spermatogonia. Immunostaining for germ cell nuclear antigen 1 (GCNA1; a marker for immature spermatogonia) and the proliferation marker Ki67 revealed no quantitative differences between WT and p73KO mice of different ages
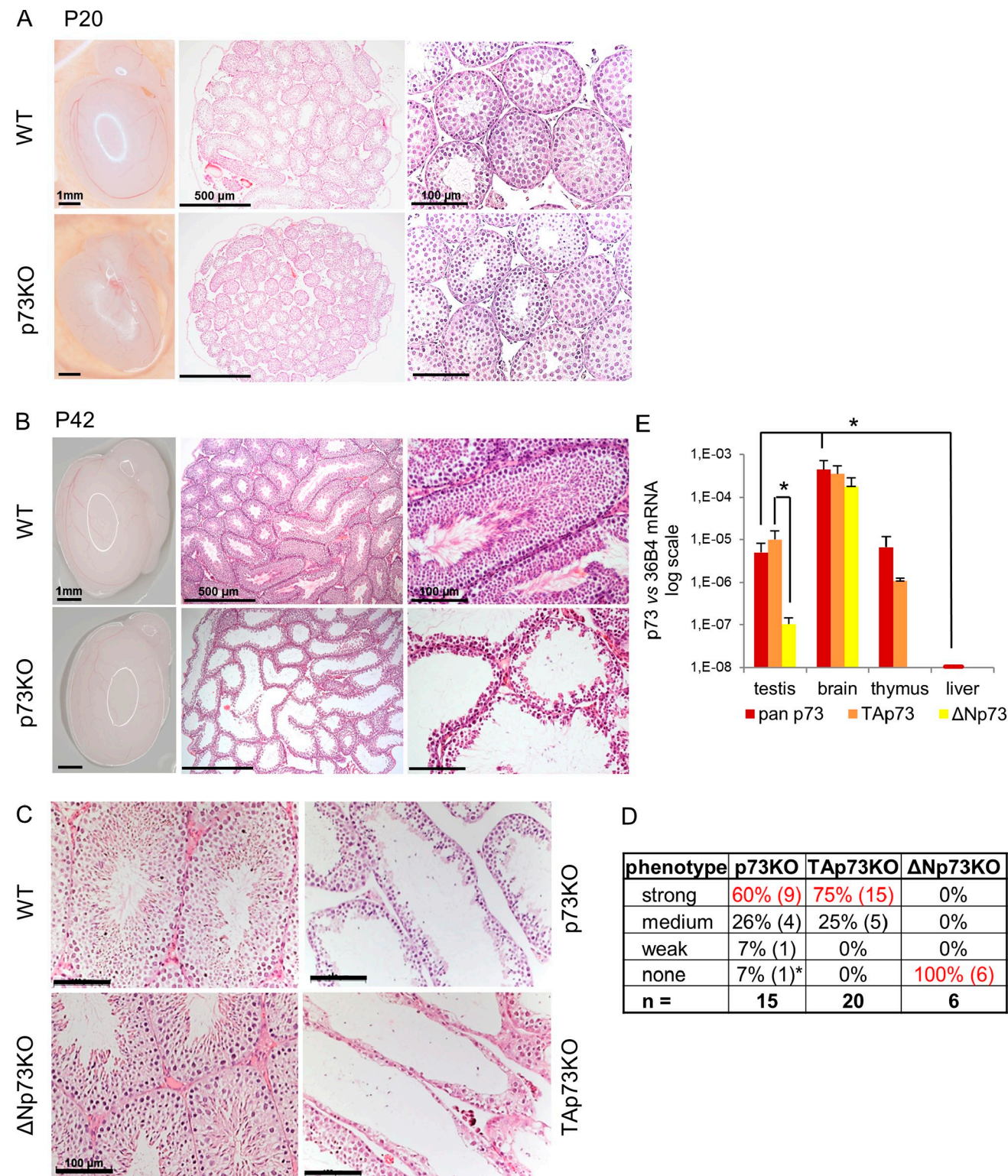
Figure 1.   **TAp73 deficiency causes a profound absence of developing and mature germ cells from the seminiferous epithelium.** (A and B) Testis histology from p73KO and WT littermates at ages P20 (A) and P42 (B). H&E staining was used. Sexually mature 6-wk-old p73KO mice (B) show severe loss of developing germ cells and mature spermatozoa, creating "nearly empty" seminiferous tubules. Some variability in severity from tubule-to-tubule in a given KO mouse or among different mice was noted. (A and B, left) Whole testis with epididymis. (C) Testis histology from adult WT, p73KO, and isoform-specific ΔNp73KO and TAp73KO mice of similar age (7–10 wk). H&E staining was used. TAp73KO mice phenocopy global p73KO mice, whereas ΔNp73 deficiency does not affect testis morphology. (D) Severity of the testicular phenotype. Shown is a summary of all analyzed mice (6–10 wk) assessed by scoring H&E sections. p73KO (86%) and TAp73KO (100%) mice show medium-to-strong loss of developing and mature germ cells and a flat germ epithelium. In contrast, all ΔNp73KO mice have normal morphology. Asterisk: compared with its littermates, this 6-wk-old p73KO animal had small testis, which indicated delayed development. (E) p73 mRNA levels in different organs of 6–10-wk-old WT mice. qRT-PCR of all (pan) or TA/ΔN-specific isoforms was performed. TAp73 is the predominant isoform in testis (>100-fold higher than ΔNp73). *n* = 2–3 per organ, mean ± SD (error bars). *, P < 0.05 (*t* test). See also Fig. S1.

Figure 2. **TAp73KO testis shows selective loss of round and elongated spermatids and spermatozoa, while spermatogonia and meiotic spermatocytes are not affected.** (A) TAp73KO mice show marked loss of the later stages of developing sperm (arrows). Immunofluorescence analysis for stage-specific markers VASA (which stains spermatocytes and round spermatids) and APG1 (which stains spermatids and spermatozoa) on testes from 10-wk-old

(Fig. 2, E–G). Also, the number of meiotic spermatocytes was normal in p73KO testis, which was confirmed by the quantitation of all nonbasal cells using the mitosis and meiosis marker phospho-H3Ser10 (Fig. 2, H and I). In sum, TAp73 loss causes depletion of mainly round and elongated spermatids and spermatozoa, while sparing basal stem-cell spermatogonia and meiotic spermatocytes.

The epididymis of TAp73KO mice indicates premature sloughing of developing germ cells from the seminiferous epithelium of testis

Next we asked whether the premature germ loss from seminiferous KO epithelium is reflected in apoptotic sperm within the testicular lumen, and also results in depletion of mature spermatozoa in the epididymis, its contiguous downstream storage organ. Indeed, the lumen of seminiferous tubules in >50% of KO mice contained TUNEL+ dead sperm, a phenotype never detected in WT mice (Fig. 3, A and D). Moreover, the caudal epididymis revealed either completely or nearly empty tubules in ∼50% of all TAp73/p73KO mice. In contrast, 100% of WT mice displayed caudal epididymis packed with mature spermatozoa (Fig. 3, B and D). Moreover, other KO mice showed TUNEL+ sperm in the cauda epididymis, which is not seen in WT littermates (Fig. 3, C and D). Loss of mature spermatozoa in the KO cauda epididymis was confirmed by decreased luminal APG1 staining, which marks late developing/mature sperm, but increased VASA staining, which marks sloughed-off early immature sperm (Fig. 3, C and D). In sum, KO germ cells appear to prematurely slough off the seminiferous epithelium and die by apoptosis, which explains the major loss of mature spermatozoa in epididymis storage and infertility of TAp73KO mice.

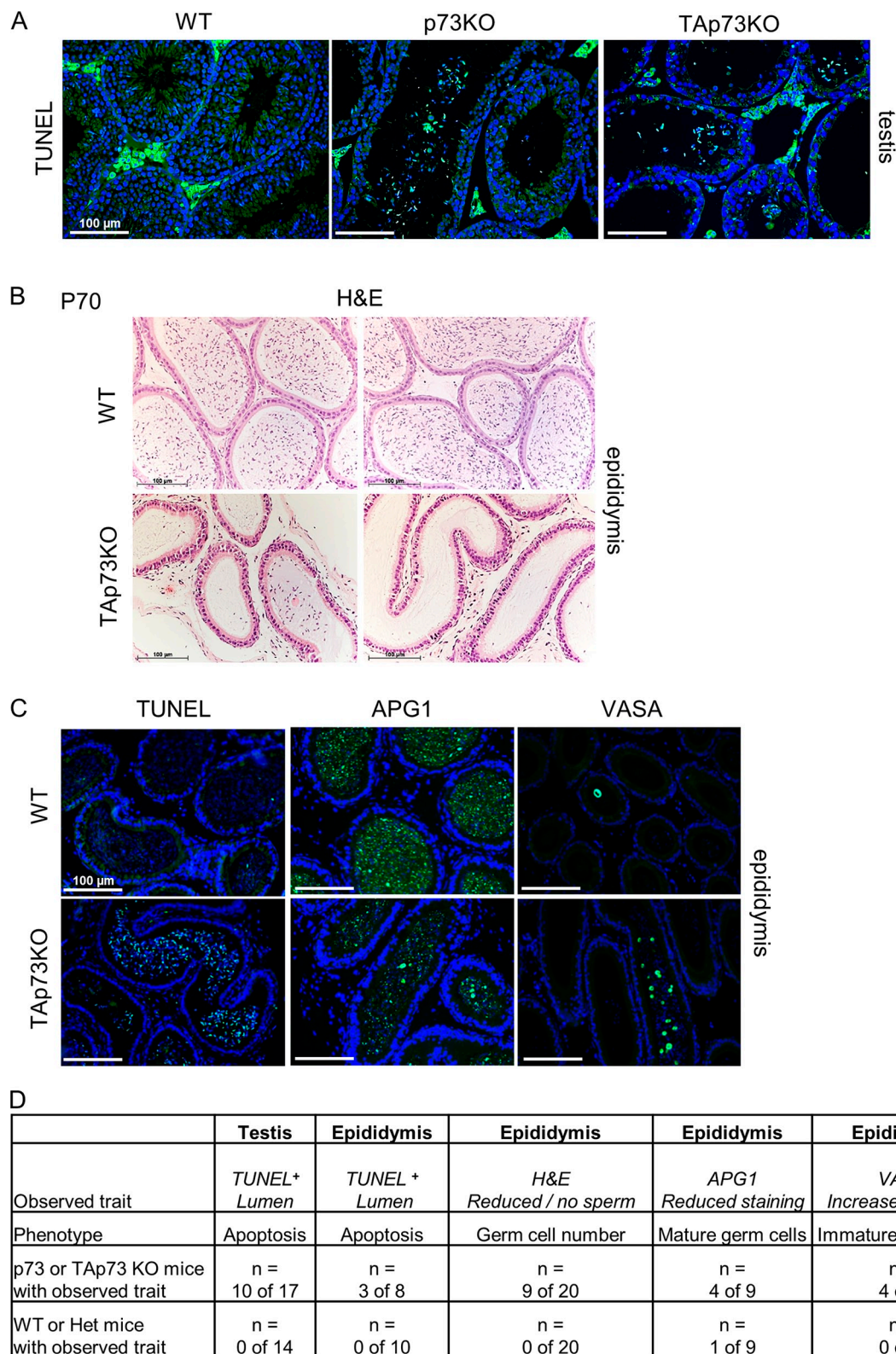### Sertoli cell morphology is degenerate in TAp73KO mice

Spermatogenesis critically depends on Sertoli cells, interspersed tall somatic cells in the germ epithelium that reach from the BM into the lumen and provide crucial structural support, nutrition, and protection for developing sperm. A single Sertoli cell provides many "floors" of intracellular nursing pockets via long cytoplasmic arms to house germ cells at different developmental stages. Thus, Sertoli cells build the highly organized cell layers of the seminiferous epithelium (Griswold, 1998). Because we observed a highly disorganized KO epithelium with strong germ cell loss, we asked whether Sertoli cells are implicated.

Immunofluorescence analysis with the nuclear Sertoli marker Wilms tumor 1 (WT1) showed no difference in cell numbers and nuclear staining patterns between KO and WT mice at 7 wk, and only a minor decrease by 10 wk of age (Fig. 4, A and B). Importantly, TAp73KO Sertoli cells exhibited marked structural abnormalities, indicated, for example, by immunostaining for the intermediate filament Vimentin, a cytoplasmic Sertoli marker (Aumüller et al., 1988). In contrast to WT, where every cell showed strong linear full-epithelial-thickness Vimentin staining, KO Sertoli cells exhibited a lack thereof because of their very short and thin cytoplasmic arms (Fig. 4, C and D). Moreover, electron microscopy analysis confirmed the defective morphology of KO Sertoli cells, revealing retracted thinned cytoplasmic arms and a marked increase in degenerative vacuolization within the cytoplasm (Fig. 4 E and Fig. S3 C). Also, the WT epithelium was characterized by tightly packed layers of developing germ cells sitting in nursing pockets of Sertoli cells with their arms closely wrapped around the germ cells. In contrast, the TAp73KO epithelium displayed a highly disorganized structure with reduced cell numbers of only loosely attached or completely detached germ cells, large irregular cavities between Sertoli–Sertoli and Sertoli–germ cells, and an aberrant vertical order of sperm development including the presence of elongated spermatids in basal layers near the BM. Conversely, the retained germ cells showed no other structural abnormalities (Fig. 4, E and F; and Fig. S3). In sum, TAp73KO testis exhibit degenerate Sertoli cell morphology, associated with disorganization of the germinal epithelium and germ cell depletion.

In the male germ line, TAp73 controls a transcriptional program of balanced cell adhesion and migration, including proteases, inhibitors of proteases and serine peptidases, receptors, and integrins

We hypothesized that these organizational defects are caused by disruption of cell–cell connections, leading to disturbed interactions between Sertoli and germ cells, and causing impaired sperm development and premature sperm loss. To gain insight into the molecular mechanism underlying the "nearly empty tubule" phenotype, we performed whole transcriptome microarray analysis on 10-wk-old TAp73KO versus WT testes ($n = 3$ mice/genotype). Surprisingly, 148 of the 159 differentially regulated genes showed up-regulation in TAp73KO germinal epithelium compared with WT. Fig. 5 A shows a heat map of the top 50 genes deregulated in TAp73KO testis. Of note, a large group (26 of 159, 16.4%)

---

littermates is shown. (B) Round (arrow) and elongated (arrow with broken line) spermatids are strongly reduced in adult p73KO testis. DAPI staining of littermates is shown. The asterisk indicates a pachytene spermatocyte. Quantitation of spermatids is also shown. $n = 4$ mice/genotype, mean ± SD (error bars); ***, P < 0.005 (*t* test). (C) p73KO mice display a 20–30% reduction in germ cell area per total seminiferous tubular area. $n = 4$–5 mice/genotype, mean ± SD (error bars); ***, P < 0.005 (*t* test). (D) p73KO testes have more tubules with low total germ cell count. $n = 5$ mice/genotype, mean ± SD (error bars); ***, P < 0.005 (*t* test). ns, not significant. (E) TAp73KO testes show normal numbers of proliferating basal spermatogonia. Immunohistochemical analysis for GCNA1 (which marks basal spermatogonia) and proliferation marker Ki67 is shown. (F) Quantitation of basal spermatogonia in 6-wk-old mice from E. GCNA1+ cells within a distance of 120 μm from the basal lamina were counted. $n = 3$–5 mice/genotype, mean ± SD (error bars), P > 0.05 (*t* test). (G) p73KO testes have normal numbers of proliferating cells. $n = 2$–5 mice/genotype/age, mean ± SD (error bars), P > 0.05 (*t* test). (H) Meiosis is intact in p73KO testis. Immunofluorescence analysis for phosphorylated H3, which marks mitotic and meiotic cells, is shown. (I) Quantitation of meiotic cells in p73KO versus WT mice of different ages. No difference in the number of H3Ser10-positive cells was detected. $n = 2$–5 mice/genotype/age. (F, G, and I) Results indicate mean ± SD (error bars), P > 0.05 (*t* test). See also Fig. S2.

A

WT   p73KO   TAp73KO

TUNEL

100 µm   testis

B P70   H&E

WT

TAp73KO   epididymis

C   TUNEL   APG1   VASA

WT

100 µm

TAp73KO   epididymis

D

|	Testis	Epididymis	Epididymis	Epididymis	Epididymis
Observed trait	*TUNEL⁺ Lumen*	*TUNEL⁺ Lumen*	*H&E Reduced / no sperm*	*APG1 Reduced staining*	*VASA Increased staining*
Phenotype	Apoptosis	Apoptosis	Germ cell number	Mature germ cells	Immature germ cells
p73 or TAp73 KO mice with observed trait	n = 10 of 17	n = 3 of 8	n = 9 of 20	n = 4 of 9	n = 4 of 9
WT or Het mice with observed trait	n = 0 of 14	n = 0 of 10	n = 0 of 20	n = 1 of 9	n = 0 of 7

Figure 3. **The epididymis of TAp73KO mice indicates premature sloughing of developing germ cells from the testicular epithelium.** (A) The lumen of seminiferous tubules of p73KO and TAp73KO mice contains numerous apoptotic sperm. TUNEL staining of adult testes is shown. Interstitial Leydig cells show unspecific staining, as hormone-producing cells frequently do. (B and C) Consequently, the lumen of the KO caudal epididymis is either nearly or completely empty (B) or contains reduced numbers of mature sperm (C; APG1, spermatids, and spermatozoa) but increased numbers of apoptotic (TUNEL) and immature sperm (VASA, spermatocytes, and round spermatids). Bar in B, 100 µm. H&E sections (B) and immunofluorescence analysis (C) from adult littermates are shown. (D) Summary of staining analysis of testis and epididymis from p73KO, TAp73KO, and WT/Het adult mice. About 50% of all KO mice show apoptotic cells within the lumina of testis and epididymis (TUNEL+). Concomitantly, nearly 50% have decreased mature sperm (H&E, APG1) but increased immature sperm (VASA) in the downstream epididymis.
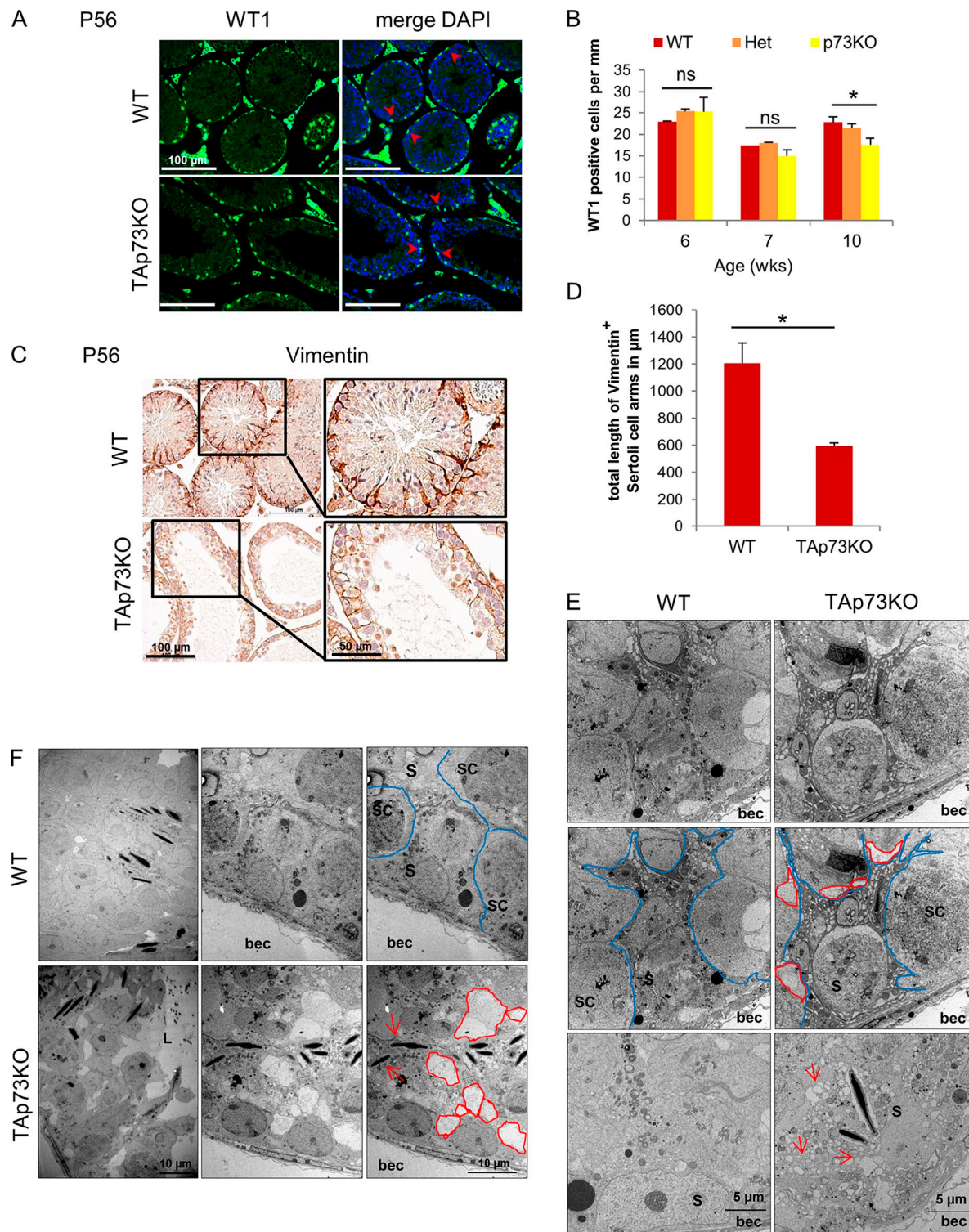
Figure 4. Sertoli cell morphology is degenerate in TAp73KO mice. (A and B) The number of Sertoli cells is normal in KO mice. Immunofluorescence analysis (A) and quantitation (B) of testis of adult TAp73KO and WT/Het mice of different ages for WT1, a nuclear Sertoli cell marker (arrowheads), is shown. Interstitial Leydig cells show unspecific staining. n = 2–5 mice/genotype, mean ± SD (error bars). ns, not significant. *, P < 0.05 (t test). (C and D) KO Sertoli cells have abnormally short and thin cytoplasmic arms. (C) Immunostaining of testis of adult TAp73KO and WT mice for Vimentin, an intermediate filament Sertoli cell marker. (D) Quantitation. The lengths of all cytoplasmic arms within a field of view reaching from the basal lamina up to the lumen were added (total length of Vimentin + Sertoli cell arms). n = 3 mice/genotype. Results are the mean ± SD (error bars) of five fields. *, P < 0.005 (t test). (E and F) Electron microscopy of adult testis of TAp73KO and WT mice. (E) KO Sertoli cells (S, outlined in blue) have abnormally thin cytoplasmic arms, high vacuolization (arrows), and poor adherence to neighboring germ cells (large lacunar gaps, outlined in red). WT Sertoli cytoplasmic arms are broad and tightly wrapped around germ cells (SC). In contrast, KO Sertoli cells show degenerate morphology. (F) In KO seminiferous epithelium, germ cells are very loosely packed and Sertoli cells fail to envelope and retain the developing gametes. Gaps and holes are marked in red. Arrows indicate elongated spermatids aberrantly close to the basal lamina. In contrast, WT epithelium is firmly packed with germ cells (SC) attaching very tightly to their Sertoli nurse cell (S, marked in blue). L, lumen; bec, basal extracellular. (E and F) Representative images from n = 9–10 mice/genotype. See also Fig. S3.
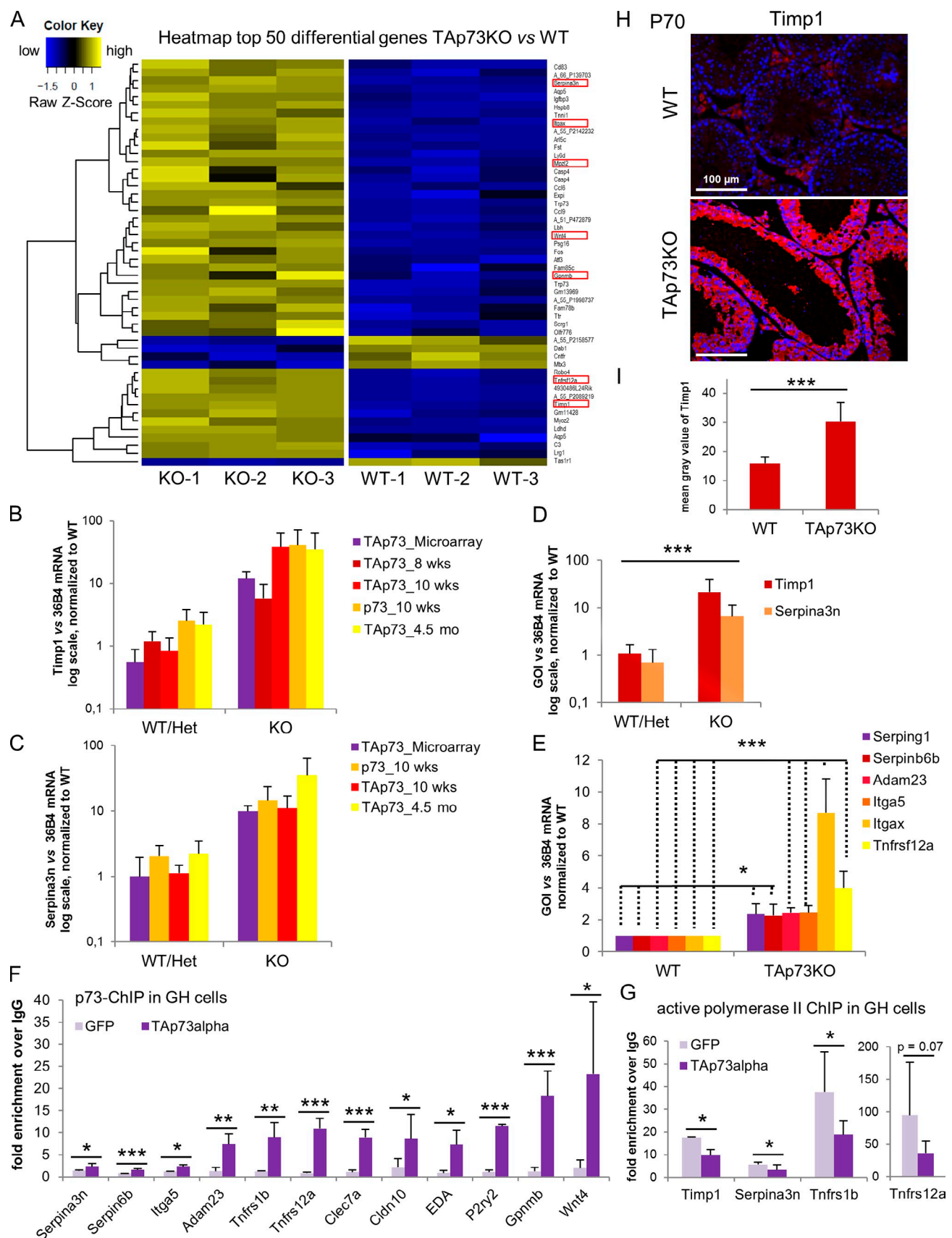
Figure 5. **In the male germ line, TAp73 controls a transcriptional program of balanced cell adhesion and migration within the germinal epithelium.** Inhibitors of proteases and serine peptidases, proteases, receptors, and integrins are dysregulated in TAp73KO testis. (A) Microarray analysis of whole testis from 10-wk-old TAp73KO versus WT littermates. *n* = 3 mice/genotype. The heat map shows the top 50 of the 159 differentially regulated genes that were

of differential genes in KO testis are associated with adhesion and migration, including protease inhibitors, serine peptidase inhibitors (Serpins; aka, plasminogen activator [PA] inhibitors [PAIs]), proteases, and integrins (Tables S1 and S2). Strongly up-regulated genes like tissue inhibitor of metalloproteinase 1 (*Timp1*) and *Serpina3n* (serine peptidase inhibitor) are expressed in testis and have a known role in regulating cell attachment and germ cell migration (Guyot et al., 2003; Siu et al., 2003; Le Magueresse-Battistoni, 2007). Validation of the microarray data by quantitative real-time PCR (qRT-PCR) confirmed the strong induction of Timp1 and Serpina3n (10–60 fold) in adult TAp73KO and p73KO compared with WT testis, independent of age (Fig. 5, B–D). Moreover, up-regulation of serine peptidase inhibitors Serping1 and Serpinb6b, surface cell contact protein Adam23, integrins Itga5 and Itgax, and tumor necrosis factor receptor Tnfrsf 12a occurred in TAp73KO compared with WT testis (Fig. 5 E). A direct transcriptional regulation of these genes by TAp73 was confirmed by several binding studies at these loci. Our published whole genome chromatin immunoprecipitation (ChIP) sequencing data in Saos-2 cells (Koeppel et al., 2011) initially revealed TAp73 binding to the human loci of *Itga5*, *Timp1*, *Serpina3n*, *Tnfrsf1b*, and *Tnfrsf12a* (Fig. S4, E–J), as well as *Adam23* and *Serpinb6b* (not depicted). Next, direct TAp73α binding to the promoters of a broad panel of these adhesion-associated genes was further validated by targeted ChIP assays in Saos-2 cells (Fig. S4, B–D) and, most importantly, in human testis–relevant GH testicular carcinoma cells (Fig. 5 F and Fig. S4 A). Moreover, in support of our microarray and ChIP sequencing data, TAp73α expression in GH cells led to their transcriptional repression, indicated by decreased recruitment of active polymerase II to their gene loci (Fig. 5 G). In sum, these in vitro data also exclude the possibility that the differential gene expression in vivo might have been caused by the skewed cell types contained in KO versus WT testes. Marked up-regulation of Timp1 protein in TAp73KO testis was confirmed by immunostaining (Fig. 5, H and I). Timp1 was strongly expressed in the cytoplasm of cells in KO germ epithelium, while hardly detectable in WT testis. In sum, TAp73 controls a transcriptional program of balanced cell adhesion and migration. Its loss leads to strong dysregulation of this balance by, e.g., up-regulation of Timp1, Serpins, proteases (matrix metalloproteases Adam23, Mmp23), integrins (Itga5, Itgax), and receptors (Tnfrsf 12a, Tnfrsf 1b). This could explain the observed germ adhesion and migration defects in TAp73KO testis.

TAp73 is exclusively expressed in germ cells and regulates germ cell adhesion to Sertoli nurse cells by modulating the germ cell transcriptional program

Because we found defective germ cell adhesion as well as aberrant Sertoli cell morphology in KO testis, we next asked which cell type expresses TAp73. To obtain specific primary populations, we used freshly isolated germ cell pellets and briefly cultured Sertoli cells at passage 0 (Ahmed et al., 2009). qRT-PCR analysis of isolated WT germ and Sertoli cells revealed that TAp73 is exclusively expressed by germ cells but not by Sertoli cells (Fig. 6 A and Fig. S5 A). Moreover, RNA in-situ hybridization for TAp73 in WT testis confirmed TAp73 expression mainly in maturing germ cells in upper layers of the epithelium, which is the stratum exhibiting the strongest cohesion phenotype (Fig. 6 B and Fig. S5 B). This suggests that the adhesion and migration defects of the TAp73KO germinal epithelium are a germ cell–autonomous phenotype. To test this hypothesis, we performed a germ cell–specific whole genome microarray analysis on freshly isolated germ cell pellets from adult TAp73KO versus WT littermates ($n = 3$ mice/genotype). The germ cell–specific heat map (Fig. 6 C) shows the top 50 of 71 differentially regulated genes that were at least twofold up- or down-regulated in KO germ cells. Of those, 12 adhesion genes (17%) had been equally up-regulated in microarray analysis from whole TAp73KO testis (Fig. 6 C, red boxes; and Table S2). Next, we used isolated high purity germ cell pellet versus Sertoli cell populations for qRT-PCR validation, as indicated by marker genes for germ (Sycp1 for meiotic spermatocytes, Odf1 for round spermatids) and Sertoli (Vimentin) cells (Fig. S5, D, F, and G).

We could specifically validate all important deregulated adhesion genes (*TIMP1*, *Serpina3n*, *Serping1*, *Serpinb6b*, *Tnfrsf12a*, *Adam23*, *Itga5*, *ItgaX*, *Wnt4*, *MMP23*, *P2ry2*, *Gpnmb*, *Clec7a*, *Spp1*, *Syk*, *Pdpn*, and *Mpzl2*) in TAp73KO germ cells (Fig. 6 D). Moreover, we detected TAp73 binding to their promoters, which was associated with reciprocally decreased PolII recruitment in GH cells (Fig. 5, F and G). Importantly, in sharp contrast, isolated WT and KO Sertoli cells showed no expression difference in any of these genes (Fig. 6 E and Fig. S5, C and E). Hence, aberrant induction of protease and peptidase inhibitors and junctional proteins occurs specifically in germ cells of the TAp73KO seminiferous epithelium. In sum, in the germinal epithelium TAp73 is specifically expressed in germ

at least twofold up- or down-regulated in KO testis. Of those, 26 genes (16.4%) are associated with adhesion and migration. Examples are highlighted. (B–D) Timp1 and Serpina3n are highly up-regulated in KO testes. Quantitation of Timp1 (B) and Serpina3n (C) mRNA in p73KO, TAp73KO, and WT testis was performed with qRT-PCR. Whole testes of mice from A (TAp73_Microarray) and additional testes from littermates of different ages were analyzed. $n = 3$–6 mice/genotype and age, mean ± SD (error bars). (D) Summary of Timp1 (B) and Serpina3n (C) expression in adult mice. GOI, gene of interest. $n = 16$–22 mice/genotype, mean ± SD (error bars). ***, $P < 0.005$ (t test). (E) Adhesion- and migration-associated genes like serine peptidase inhibitors *Serping1* and *Serpinb6b*, metallopeptidase *Adam23*, integrins *Itga5* and *Itgax*, and TNF receptor *Tnfrsf12a* are up-regulated in KO mice. Quantitation of mRNAs from adult TAp73KO and WT testis via qRT-PCR is shown. $n = 3$ mice/genotype, mean ± SD (error bars). *, $P < 0.05$; ***, $P < 0.005$ (t test). (F) Validation of direct TAp73α binding to promoters of adhesion-related genes. ChIP assays were performed on chromatin from GH testicular carcinoma cells transiently expressing TAp73α. Binding is quantitated as fold enrichment over IgG, comparing control (GFP)- and p73-transfected cells. $n = 3$ independent samples, mean ± SD (error bars). *, $P < 0.05$; **, $P < 0.01$; ***, $P < 0.005$ (t test). (G) Binding of active Polymerase II to the indicated genes in targeted ChIP assays in GH cells. Upon TAp73α expression, transcription of several genes including *Timp1*, *Serpina3n*, *Tnfrsf1b*, and *Tnfrsf12a* is repressed due to decreased PolII binding. Binding is quantitated as fold enrichment over IgG, comparing control (GFP)- and p73-transfected cells. $n = 3$ independent samples, mean ± SD (error bars). *, $P < 0.05$ (t test). (H) Seminiferous epithelium of TAp73KO mice expresses greatly elevated levels of Timp1. Immunofluorescence of adult testis is shown. Interstitial Leydig cells show unspecific staining. (I) Quantitation of Timp1 staining in H. $n = 5$–7 mice/genotype, mean ± SD (error bars). ***, $P < 0.005$ (t test). See also Fig. S4 and Tables S1 and S2.
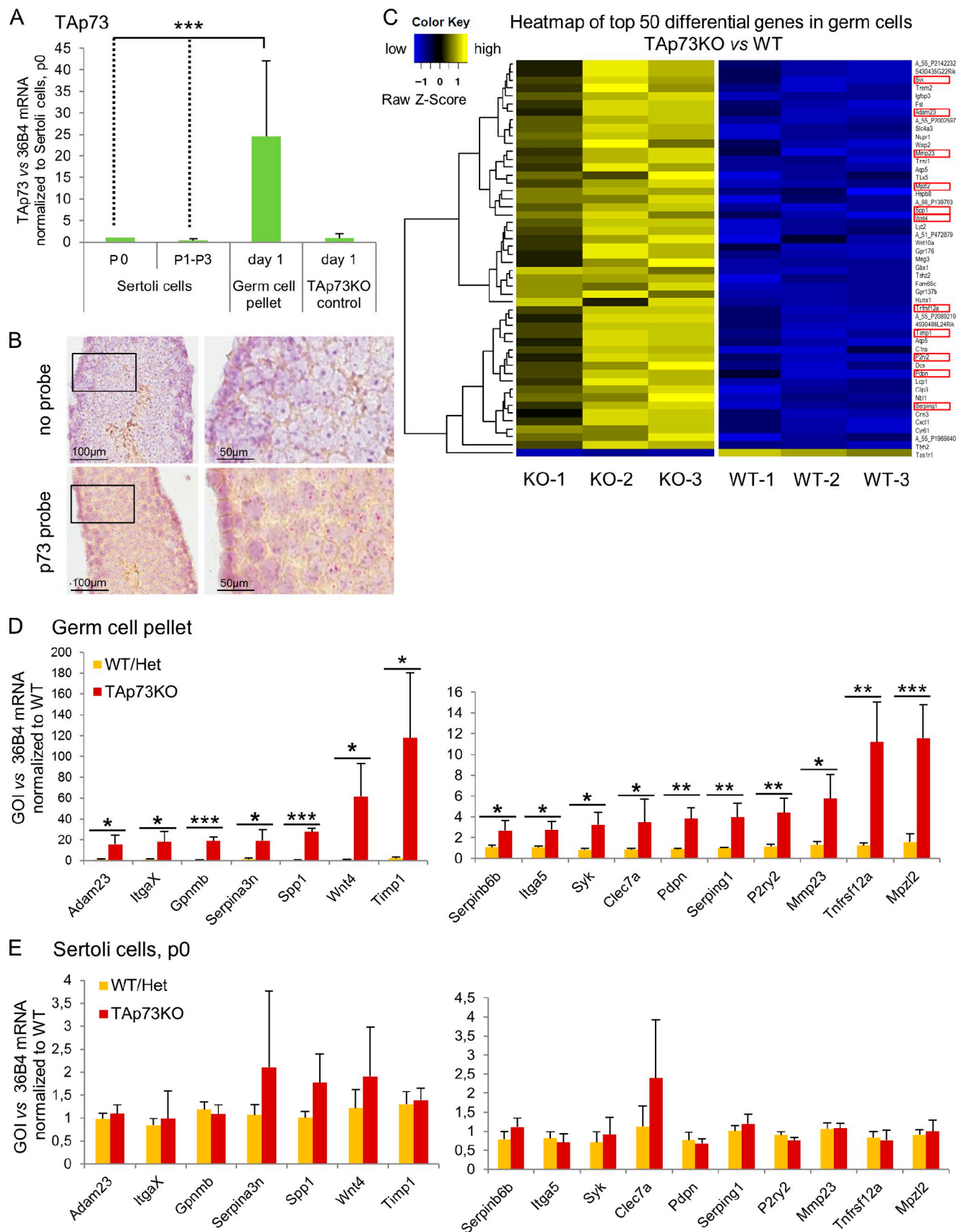
Figure 6. **TAp73 is exclusively expressed in germ cells and regulates germ cell adhesion onto Sertoli cells by modulating the transcriptional program of germ cells.** (A) TAp73 is exclusively expressed in germ cells, whereas Sertoli cells have undetectable levels independent of passaging (P0–P3). The germ cell fraction of TAp73KO testis served as a negative control. qRT-PCR, n = 5–10 independent fractions each, mean ± SD (error bars). ***, P < 0.005 (t test).

cells, where it is required for expression of adhesion and migration proteins.

To test whether these TAp73-controlled genes indeed have a functional role in the germ–Sertoli adhesion process, we next performed in vitro and in vivo adhesion assays using lentiviral coexpression of five representative deregulated genes (Mix of *Serpina3n*, *Timp1*, *Itga5*, *Serping1*, and *Tnfrsf12a*; Fig. 7 A) plus lenti-GFP, versus lenti-GFP alone. As shown in Fig. 7 (B–D), classic co-cultures of Sertoli cells with Mix+GFP-transduced germ cells from WT rats (Aravindan et al., 1996) reproducibly yielded much fewer adherent germ cells compared with GFP-only transduced controls. Moreover, intraluminal lentiviral injections of Mix+GFP into the seminiferous tubules of WT testis retrograde via the efferent ductules (Ogawa et al., 1997) reproduced the germ cell discohesion phenotype in many tubules, whereas GFP-only lentiviral control injections failed to do so (Fig. 8). In sum, these data indicate that deregulation of these genes plays a causal role in the mutant testis.

TAp73 loss results in structural cell–cell junction defects and severe disruption of the BTB in the germinal epithelium

The dysregulation of an adhesion and migration program in TAp73KO mice appears to be the molecular basis of their testicular phenotype and infertility. This functional group of proteins, when expressed at normal balanced levels in WT testis, supports a complex and dynamic upward migration. Before entering meiosis, germ cells first have to cross the physical barrier generated by specific basal Sertoli–Sertoli cell junctions. These basal tight junctions form the critical structural element of the BTB, which ensures strict separation of the mitotic stem cell compartment from the meiotic and postmeiotic compartment (Yan et al., 2007), and physically protects developing germ cells from circulating endogenous autoantigens and toxins (Xia et al., 2005). To build BTB tight junctions, an array of paired actin bundles of two adjacent Sertoli cells have to be anchored directly opposite of each other (Fig. 9 A, WT). Notably, electron microscopy analysis of KO seminiferous tubules revealed impaired junctional BTB structures. In contrast to mirrored bilateral WT structures, TAp73KO tubules displayed aberrant one-side-only tight junctions, with the opposing actin bundles of the adjacent Sertoli cell missing or side-shifted from the junctional complex (Fig. 9 A). To test the functionality of the BTB barrier, we performed the classic in vivo biotin assay in TAp73KO and WT mice. Biotin was carefully injected at low pressure into the center of the testis, and after lymphatic diffusion (30 min) its extracellular distribution within the seminiferous epithelium was measured by staining tissue

sections with Streptavidin-coupled Texas red. As expected, WT testis showed sharply delineated staining, outlining only the very basal spermatogonial but not the upper cell layers (Fig. 9 B, smallest bracket). In sharp contrast, in TAp73KO testis biotin readily infiltrated the full thickness of the germ epithelium (Fig. 9 B, larger brackets). The staining intensity in TAp73KO testis, reflecting the degree of BTB defects, was directly proportional to the severity of pathological sloughing within a given section of seminiferous epithelium (Fig. 9 C). In addition to severe BTB defects at the base, we observed structural defects in cell–cell junctions between Sertoli and germ cells suprabasally (unpublished data). Finally, the apical ectoplasmic specialization (ES), an adherens junction–like structure, is formed between Sertoli cells and apical spermatids (Lee and Cheng, 2004). In TAp73KO testis, immunostaining for Espin, a specific microfilament-binding protein of the apical ES (Bartles et al., 1996), revealed irregular short, thin Espin-positive junctions, contrasting with the highly organized thick palisading ES structures in WT mice (Fig. 9 D).

In sum, these data support a marked cell-autonomous adhesion, migration, and maturation defect of germ cells in TAp73KO testis. At its core, cell–cell adhesions of developing germ cells to their Sertoli nurse cells are severely disrupted. The degenerative morphological changes of Sertoli cells including loss of the BTB are likely a secondary consequence, triggered by the discohesion of germ cells. Mechanistically, loss of TAp73 in germ cells leads to transcriptional dysregulation, destroying the careful balance between proteases (matrix metalloproteinases [MMPs], PAs) and their inhibitors (Timp1, Serpins), integrins, and receptors. As a consequence, the formation of basal Sertoli–Sertoli and suprabasal germ cell-Sertoli junctions is severely disturbed, leading to massive premature sloughing of immature germ cells from the germ epithelium. This is the pathological basis of male infertility of TAp73KO mice (Fig. 9 E).

Discussion

Here we identify an unexpected role of TAp73 as an essential factor enabling the adhesion and maturation of germ cells in adult testis. Depletion of TAp73, but not ΔNp73, leads to premature sloughing of developing germ cells from the seminiferous epithelium. While basal proliferating spermatogonia and meiotic spermatocytes are largely preserved, later-stage spermiogenic cell layers are strongly depleted in KO mice. The flattened KO epithelium is characterized by defective cell–cell contacts, with major structural abnormalities of Sertoli–Sertoli junctions including the BTB and Sertoli–germ cell junctions. Moreover, large lacunar gaps are common between the (normally tightly enveloped) germ

---

See also Fig. S5 A. (B) RNA in situ hybridization for TAp73 in WT seminiferous tubules. Signal intensity for TAp73mRNA (pink dots) is strongest in the upper germ layers containing maturing germ cell stages, and weaker in the basal part of the epithelium, which harbors stem and immature germ cells and Sertoli cell bodies. Both magnified panels (enlarged on the right) are also shown in Fig. S5 B. (C) Germ cell–specific microarray analysis from freshly isolated germ cells of adult TAp73KO versus WT littermates. n = 3 mice/genotype. The heat map shows the top 50 of 71 differentially regulated genes that were at least twofold up- or down-regulated in KO germ cells. 12 adhesion genes (17%, red boxes) are equally up-regulated in whole TAp73KO testis microarray. See also Table S2. (D and E) Only TAp73KO germ cells exhibit deregulation of a broad panel of adhesion-associated genes including *TIMP1*, *Serpina3n*, *Serping1*, *Serpinb6b*, *Tnfrsf12a*, *Adam23*, *Itga5*, *ItgaX*, *Wnt4*, *MMP23*, *P2ry2*, *Gpnmb*, *Clec7a*, *Spp1*, *Syk*, *Pdpn*, and *Mpzl2*. qRT-PCR validation of microarray results from Fig. 6 C and Fig. S5 C in freshly isolated germ cells (D) versus isolated Sertoli cells (p0; E) from TAp73KO and WT mice (n = 3). In contrast, expression levels were not changed in KO Sertoli cells (*t* test was not significant). qRT-PCR, n = 3 independent fractions/cultures, mean ± SD (error bars). *, P < 0.05; **, P < 0.01; ***, P < 0.005 (*t* test).
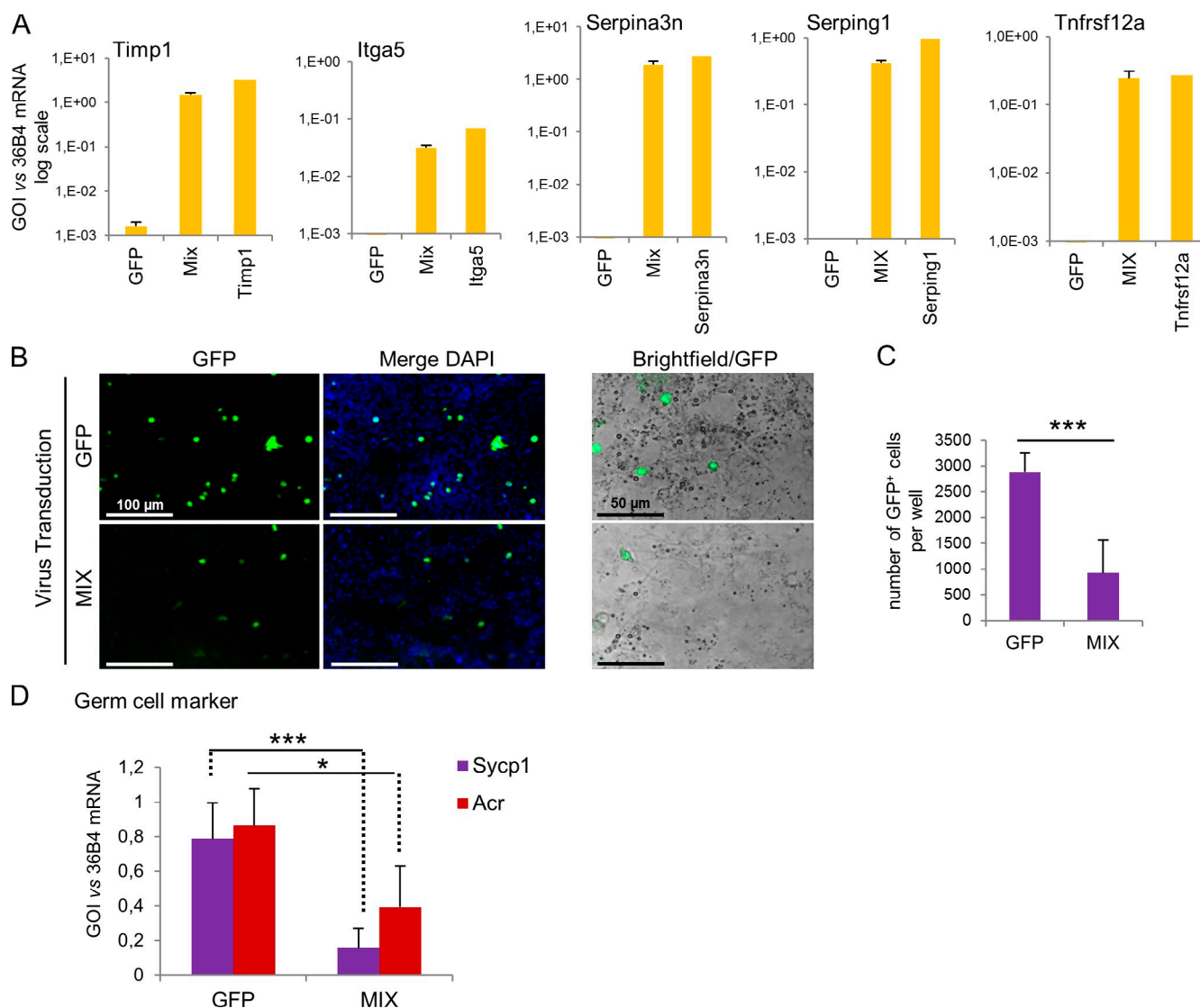
Figure 7. **The TAp73-controlled transcriptional program of adhesion-related proteins is required for germ–Sertoli cell adhesion.** Functional adhesion assays were performed in vitro. (A) Expression validation of the indicated genes in WT rat germ–Sertoli cell co-cultures 3 d after infection with lentiviral GFP alone or lentiviral five adhesion gene mix plus GFP. All wells received identical numbers of GFP virus particles and cell components. Individual lentiviral gene expression was used as a control (right bars). Representative data from three experiments is shown, mean ± SD (error bars). (B–D) Wells from A were gently washed. Then cells were fixed, counterstained with DAPI, and analyzed for GFP by microscopy (B) and Celigo quantification (C). Results indicate mean ± SD (error bars). ***, P < 0.005 (*t* test). The number of GFP-positive cells (mostly adherent immature germ cells) was markedly down-regulated after overexpression of the five gene mix. (D) Wells were also quantified by germ-specific markers (meiotic spermatocytes: Sycp1, Acr) via qRT-PCR for the amount of adherent germ cells. Results show mean ± SD (error bars). *, P < 0.05; ***, P < 0.005 (*t* test).

and Sertoli cells, severely disrupting the Sertoli nursing pockets. Thus, KO germ cells fail to firmly attach to nursing Sertoli cells, which provide essential support during their maturation. Contact loss between germ and Sertoli cells also leads to germ apoptosis and partial phagocytosis by Sertoli cells (Mruk and Cheng, 2004). In agreement, KO cauda epididymis contains an excess of dead and immature sperm or is depleted of mature sperm. The few germ cells that escape this fate and do mature are fully functional, as indicated by the fact that some KO males are only subfertile rather than sterile. This further supports the notion that the primary KO defect is the disrupted adhesive function of TAp73, and is not intrinsic to germ cells. Thus, the underlying pathology of TAp73KO testis is as follows: germ cells are produced normally, but due to severe contact and retention failure get depleted

during their upward maturational journey through the seminiferous epithelium.

We find that TAp73, which is produced by germ cells, controls a transcriptional program of balanced cell adhesion and migration by regulating a set of genes including peptidase and protease inhibitors, metalloproteases, receptors, and integrins that are critical for the dynamic adhesion and junctional restructuring processes in the germ epithelium. Timp1 was previously found expressed mainly in Sertoli but also in germ cells (Robinson et al., 2001; Mruk et al., 2003), and serine proteases (PAs) and Serpins were found in Sertoli, Leydig, and germ cells of adult testis (Charron et al., 2006; Odet et al., 2006; Sipione et al., 2006). Timp1 and Serpins are also associated with adhesion and migration during testis development. Timp1 expression increases during
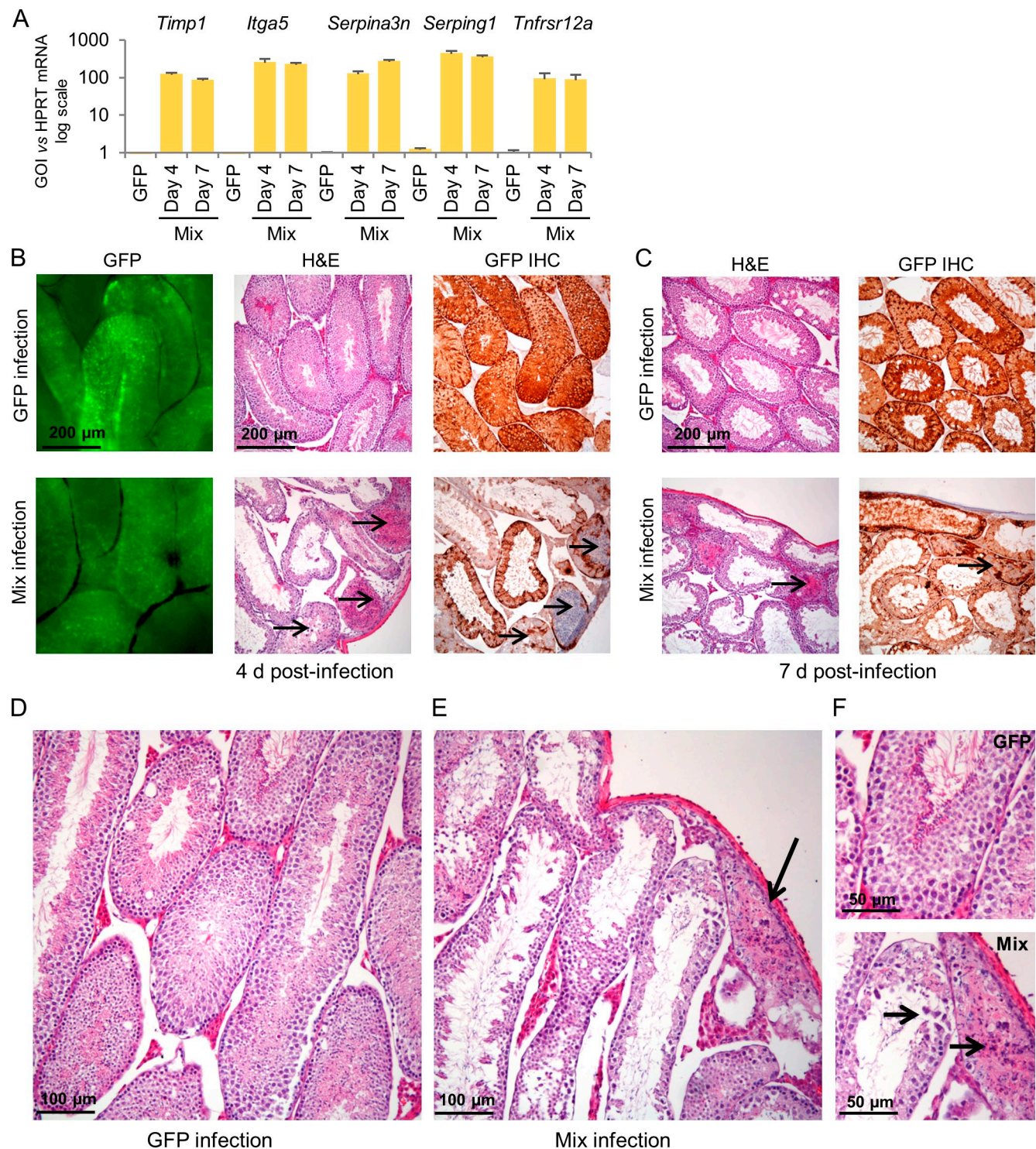
Figure 8. **Deregulated expression of TAp73-controlled adhesion-associated proteins phenocopies TAp73 testis in vivo.** Concentrated lentiviral supernatants of the five-gene mix plus GFP, or GFP alone, from Fig. 7 were injected intraluminally into the seminiferous tubules of WT testis via the efferent ductules. 4 and 7 d later, mice were sacrificed and testes were processed for qRT-PCR (A), H&E, and GFP immunostaining (B–F) to verify expression. Error bars indicate mean ± SD. (B, left) GFP expression of unfixed testes under fluorescence microscopy. $n = 4$ and $n = 5$ testes per group for day 4 and day 7, respectively. In contrast to GFP control, the five-gene mix reproduced the germ cell discohesion phenotype in many tubules (arrows).

tight junction assembly in cultured Sertoli cells and adherens junction assembly between Sertoli and co-cultured germ cells (Mruk et al., 2003). Also, Timp1 is required to counterbalance TNF-mediated activation of MMP-9 matrix metalloprotease, leading to collagen cleavage that perturbs Sertoli tight junctions (Siu et al., 2003). Serine protease activity also increases during assembly of adherens Sertoli–germ cell junctions (Mruk et al., 1997). Moreover, Serpin E1 (PAI-1) is expressed by early spermatids and Sertoli cells, and, notably, disrupts cell adhesion by competing with serine proteases for their receptors
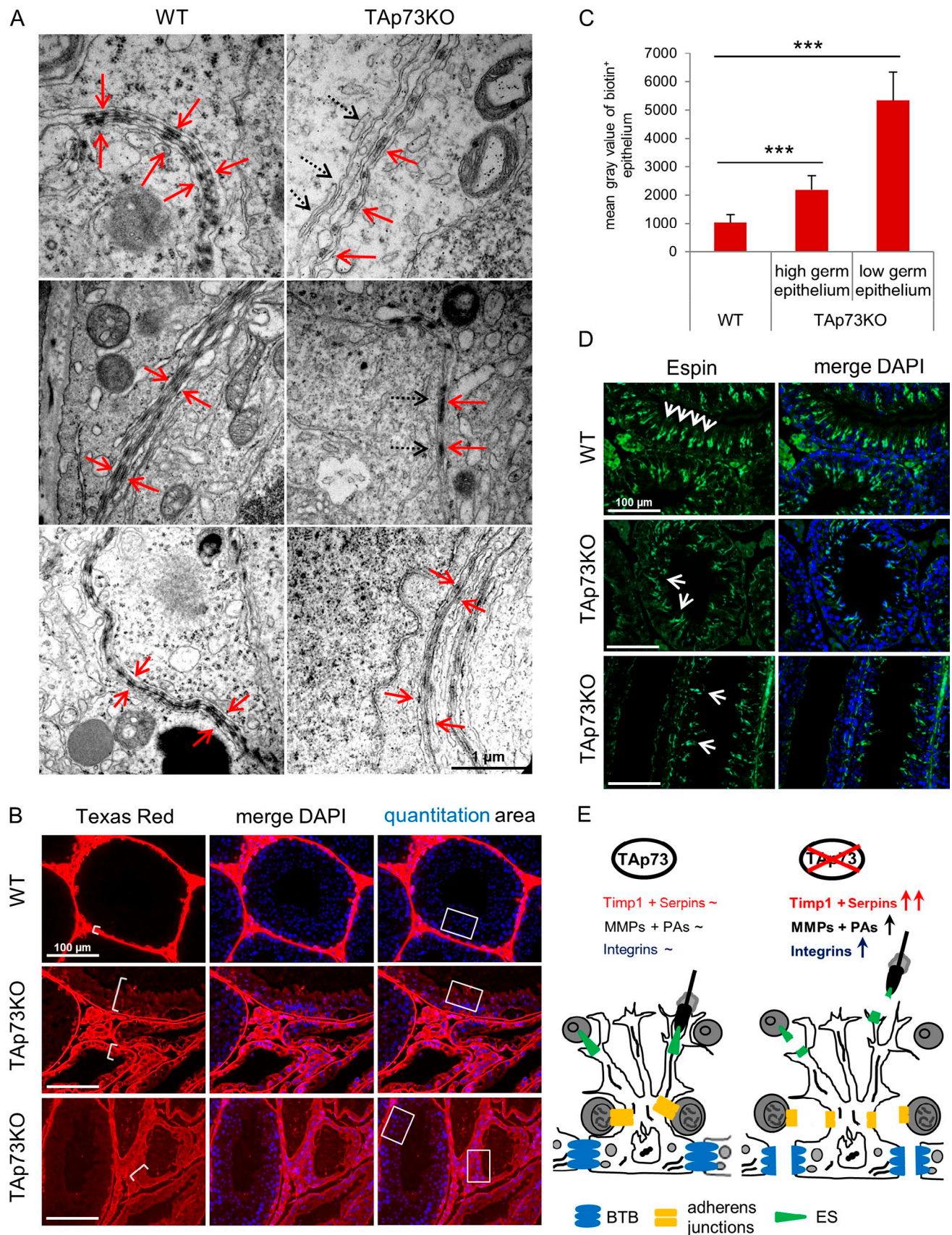
Figure 9. **TAp73 loss causes basal and apical cell–cell junction defects within the seminiferous epithelium and severe disruption of the BTB.** (A) Tight junctions of the basal BTB, formed by adjacent Sertoli cells. KO Sertoli cells show defective bilateral junctions, with only one-sided junctional structures (solid arrows) and uneven distribution of the anchoring actin bundles along the membrane contact. Broken arrows indicate the missing counterparts of the aberrant unilateral

(Le Magueresse-Battistoni et al., 1998). Our study found that TAp73 is the upstream master regulator that physiologically orchestrates the dynamics of cell–cell junctions and cell adhesions within the germ epithelium. Thus, deregulation of protease and peptidase inhibitors (like *Timp1* and *Serpins*) and other adhesion-associated genes (like *integrinα5*, *integrinαX* and *Adam23*, *Mmp23*) as a direct result of TAp73 loss can lead to an imbalance between cell-detaching proteolysis and cell-reattaching restructuring events as the molecular basis for the observed testicular phenotype.

A core evolutionary function of the p53 family is germ line quality control, i.e., protecting their genomic fidelity by eliminating damaged gametes (Coutandin et al., 2010). The invertebrate p53 orthologues CEP-1 (*Caenorhabditis elegans*) and Dmp53 (*Drosophila melanogaster*) control gamete apoptosis in response to DNA damage (Derry et al., 2001; Schumacher et al., 2001). This primary role of the p53 family is maintained from sea urchins to mammals. In mice and humans, (G)TAp63 is the preeminent protector of the male and female germ line, where it is highly expressed and becomes activated by DNA damage to ensure the genetic integrity of sperm and oocytes by inducing apoptosis (Suh et al., 2006; Guerquin et al., 2009; Beyer et al., 2011). p63 also regulates male germ cell apoptosis in fetal development (Petre-Lazar et al., 2007). p53 influences apoptosis in prenatal oogenesis during oocyte selection in prophase I of meiosis (Ghafari et al., 2009) and contributes to developmental apoptosis of prenatal sperm cells (Matsui et al., 2000). p53 also participates in removing damaged sperm in the adult, with p53KO mice retaining abnormal giant sized sperm after irradiation (Beumer et al., 1998).

Likewise, TAp73 influences the ovulation process and spindle dynamics during meiosis in developing oocytes. TAp73 loss in female mice induces spontaneous spindle abnormalities and multinucleated blastocysts (Tomasini et al., 2008). However, in contrast to its protector role in oocytes, we find that in the male germ line TAp73 does not affect the meiotic process or safeguard genomic fidelity. Instead, it is essential to ensure proper sperm maturation via the Sertoli network, orchestrated by TAp73 expression in germ cells throughout adult life.

It is of note that in somatic tissues p63 and p73 have mutually exclusive functions with no apparent overlap. p73 is indispensable for brain development, whereas p63 is completely dispensable (Yang et al., 2000; Talos et al., 2010; Holembowski et al., 2011). Conversely, p63 is crucial for stratified epithelial

morphogenesis and maintenance of epithelial stem cells, whereas p73 plays no role (Yang et al., 1999). In contrast, we propose the testis as a unique organ requiring all three family members with a strict intra-organ division of labor among them: p63 and p53 ensure germ line fidelity, whereas TAp73 ensures the production of fertile mature sperm via a complex adhesive function.

Materials and methods

Mice and rats
TAp73KO, p73KO, and corresponding WT mouse strains were bred in the mouse facility of the European Neuroscience Institute in Göttingen. p73KO mice contain a replacement of exons 5 and 6 of the Trp73 gene, which encode the DNA-binding domain, with the neomycin-resistance gene, as described in Yang et al. (2000). TAp73KO mice contain a deletion of exons 2 and 3 of the Trp73 gene, which selectively abolishes expression of all TAp73 isoforms, as described in Tomasini et al. (2008). ΔNp73KO mice contain a cassette encoding Cre and EGFP inserted in frame with the start codon of ΔNp73 in exon 3 prime, which selectively abolishes all isoforms of ΔNp73 (Tissir et al., 2009). p73KO mice were a gift from F. McKeon (Genome Institute of Singapore, Singapore; Yang et al., 2000) and TAp73KO mice were a gift from T. Mak (Princess Margaret Cancer Centre, Toronto, Ontario, Canada; Tomasini et al., 2008). TAp73KO mice were enriched for C57BL/6J background for at least six generations, and p73KO mice were enriched for SV129 background for seven generations. Both strains were maintained through interbreeding of Het mice. ΔNp73KO and corresponding WT tissue samples were provided by A. Goffinet (University of Louvain Medical School, Brussels, Belgium; Tissir et al., 2009). The study was approved by Göttingen University Animal Care Committee, and animal use was in full compliance with institutional guidelines. The BTB test was conducted at Stony Brook University and approved by its Institutional Animal Care Committee. P20 and adult Wistar rats were obtained from Charles River Laboratories.

Tissue preparation
Mice and rats were euthanized with CO_2. Testis and epididymis were removed. For RNA analysis, tissue was snap frozen in liquid N_2. For histological analysis, tissues were fixed overnight in 4% paraformaldehyde or in 2.5% glutaraldehyde/cacodylate buffer for electron microscopy analysis.

Histology and immunostaining
Paraffin-embedded 3-μm sections were processed and stained with H&E. Immunohistochemistry and IF staining were performed using standard protocols. In brief, tissue sections were rehydrated by a descending xylol-isopropanol series and subjected to antigen retrieval by boiling the tissue for 15 min in 10 mM citrate buffer, pH 6.0. Unspecific binding sites were blocked with 10% FCS/PBS (immunohistochemistry [IHC] and IF) for 30 min at room temperature, and endogenous peroxidase (IHC) was blocked by applying a 3% hydrogen peroxide solution for 10 min. Sections were incubated with the primary antibody for 16 h at 4°C. The following antibodies were used: APG1 (1:200, N-96, sc-6242, rabbit anti–mouse; Santa Cruz Biotechnology, Inc.), VASA (1:1,000, ab13840, rabbit anti–human; Abcam), GCNA1 (1:400, rat), Espin (1:400, clone 31.611656, mouse anti–rat; BD), Ki67 (1:25, M7249, rat anti–mouse; Dako), phosphoH3Ser10

junctions in KO mice. Representative electron microscopy is shown of testes from TAp73KO and WT mice, $n = 3–5$ mice/genotype. (B) The in vivo biotin assay measures the functionality of the BTB in adult WT and TAp73KO mice. Biotin distribution is visualized by Texas red staining. The intact BTB in WT testis sharply outlines only the basal cell layer (smallest bracket) because it blocks biotin from crossing into the spermatocyte and higher cell layers. In contrast, KO testes display diffuse staining throughout all layers of the seminiferous epithelium (larger brackets), which indicates a severe BTB defect with leakiness. (C) Quantitation of Texas red staining from B. Measurements within standardized areas are shown (rectangles in B). The mean gray intensity increases proportionally to the decrease in height of the germinal epithelium. $n = 4–7$ mice/genotype, 3–5 images each. Results show mean ± SD (error bars). ***, $P < 0.005$ (*t* test). (D) Apical cell–cell junctions between Sertoli and germ cells, called ES, are visualized by IF staining with the ES marker Espin. In contrast to the high-density regular palisading ES structures in WT testis, TAp73KO testes show reduced interaction points between the two cell types and a strongly disorganized ES structure (arrows). Individual mice vary in severity. $n = 5$ mice/genotype. (E) An essential adhesion function of TAp73 in ensuring maturation of germ cells (spermiogenesis) during spermatogenesis. TAp73 is expressed in germ cells and there controls a coordinated transcriptional program. Upon loss of TAp73, the balance (indicated by the tildes) of protease inhibitors (Timps, Serpins) and proteases (MMPs, PAs), integrins, and receptors is lost due to broad dysregulation of these adhesion- and migration-associated effectors. Normally they play a critical role in the coordinated homeostasis of adhesion versus migration and the cyclical disassembly versus reassembly of BTB and Sertoli–germ cell junctions to allow the upward migration of germ cells on their maturational journey to the tubular lumen. Loss of TAp73 leads to defective BTB, as well as other junctional defects and defective cell adhesion, which result in a massive loss of immature germ cells from the seminiferous epithelium. Thus, TAp73 ensures fertility by enabling sperm maturation.

Alexa Fluor 488 conjugate (1:100, 9708, rabbit anti–human; Cell Signaling Technology), Timp1 (1:10, AF980, goat anti–mouse; R&D Systems), Vimentin (1:100, sc-7557-R, rabbit anti–human; Santa Cruz Biotechnology, Inc.), and WT1 (1:300, ab15249, rabbit anti–human; Abcam). For IHC staining, a biotinylated secondary antibody (1:500, goat anti–rat or anti–rabbit; GE Healthcare) was applied for 45 min at room temperature, followed by a 1-h incubation with ExtrAvidin-Peroxidase (1:1,000, E2886; Sigma-Aldrich). Sections were stained using DAB (Carl Roth) and nuclei were counterstained with hematoxylin. For IF staining, fluorescence-labeled secondary antibodies (1:500, goat anti–rabbit Alexa Fluor 488, goat anti–mouse Alexa Fluor 488, and donkey anti–goat Alexa Fluor 594) were used. Nuclei were counterstained with DAPI (Sigma-Aldrich). TUNEL staining was done with an in situ cell death detection kit (Roche). Images were acquired on a modular microscope (AxioScope A1) with a camera (AxioCam MRc) and confocal microscope (LSM 510; all from Carl Zeiss). Images were quantified with the AxioVision Rel. 4.8 software (Carl Zeiss).

Electron microscopy
After postfixation in 1% OsO_4 and staining with 1% uranyl acetate, tissue was dehydrated and embedded in Agar 100. 30–60-nm sections were counterstained with methanolic uranyl acetate and lead citrate, and examined with a transmission electron microscope (CM120 BioTwin; Philips). Images were taken with a 1,000 × 1,000 slow scan charge-coupled device camera (Olympus).

Functional in vivo biotin assay for BTB
The classic assay from Nalam et al. (2009) was performed in 8–9-mo-old mice. Biotin (Thermo Fisher Scientific) was carefully injected at low pressure into the center of the testis. After lymphatic diffusion (30 min), its extracellular distribution within the seminiferous epithelium can be measured because biotin reacts nonspecifically with all primary amines of surface proteins forming permanent amide bonds. It is visualized by staining tissue sections with Streptavidin-coupled Texas red (1:100, 594 nm; EMD Millipore). DAPI was used as a counterstain.

Image analysis and quantification
Image analysis and quantification of IHC and IF sections was performed with the AxioVision Rel. 4.8 software, using its counting and measurement tools. For quantitation of spermatid numbers, five random tubules of DAPI-stained sections were counted (n = 4 mice each). For quantitation of germ cell mass relative to tubule area, eight tubules of H&E-stained sections per genotype (n = 4–5 mice each) were analyzed. The distribution of tubules with a defined germ cell amount (low, 1–3; medium, 4–5; high, ≥6 cell layers of the seminiferous epithelium) within three different areas per H&E section (n = 5 mice) was calculated as a percentage. For GCNA1 quantitation, the number of basally located GCNA1-positive spermatogonia per 120-µm length was measured in 10 unit lengths per mouse (n = 3–5 mice per genotype). To determine the proliferation rate of basal cells, three separate sections per mouse (n = 2–5 mice per genotype) were analyzed for Ki67-positive tubules. The meiotic rate was calculated by counting the total number of H3Ser10-positive, nonbasal cells per section in three separate sections per mouse (n = 2–5 mice per genotype). The relative number of Sertoli cells was determined by counting WT1-positive cells per tubular length, analyzing 20–25 tubules per mouse (n = 2–5 mice per genotype). The sum of all cytoplasmic Sertoli cell arms (as total length in micrometers) reaching from the BM up to the tubular lumen was calculated in Vimentin-stained testicular sections (5–10 separate areas at 200×; n = 3 mice per genotype). To determine the staining intensity of Timp1- and biotin-Texas red–positive tubules, IF sections were analyzed with Photoshop CS5 (Adobe). The mean gray value within a fixed size area of the seminiferous epithelium was determined for 3–5 images (n = 4–7 mice per genotype). For quantitation of the biotin–Texas red staining, the seminiferous epithelium was additionally classified into low (1–3 cell layers) and high germ epithelium (>3 layers). For all quantifications, the mean value of mice from the same genotype was calculated, and WT and KO mice were compared with a Student's t test.

Primary Sertoli cell culture from mice
To obtain Sertoli cells for primary culture, testes of adult mice were decapsulated in HBSS and seminiferous tubules were dispersed by collagenase/hyaluronidase/DNase-HBSS solution for 20 min at 37°C. After washing with PBS, an additional digestion step was performed with trypsin for 15 min at 37°C. The tubular pellet was washed with PBS and Sertoli cells were freed from the seminiferous epithelium by resuspending the pellet in DMEM/F12. Debris and the main germ cell fraction

were pelleted at 300 g, retaining the germ cell pellet for mRNA analysis. The final Sertoli cell–enriched supernatant was seeded into 6-well plates and cultured at 34°C with 5% CO_2 in DMEM/F12/5% FCS. During primary culture, contaminating germ cells were removed by hypotonic shock. Pure Sertoli cells at P0 were obtained after 6 d of culturing. To check for purity and to compare Sertoli cell morphology of TAp73KO and WT samples, images of different passages of Sertoli cells were taken with a microscope (Axiovert 40 CFL/AxioCam ICm1; Carl Zeiss). For IF staining, cells were fixed and stained for Vimentin plus Alexa Fluor 488.

Germ–Sertoli cocultures: In vitro and in vivo adhesion assays
For in vitro assays, Sertoli cells were obtained from P20 Wistar rats as described by Mruk and Cheng (2011). Testes were removed, decapsulated, and cut to pieces. After three washing steps (800 g, 2 min) with DMEM/F12 to remove contaminating blood cells, testis tissue was subjected to digestion with trypsin/DNase (1 mg/ml, 20 µg/ml) for 30 min at 35°C to release Leydig and interstitial cells. Another digestion step with DNase (20 µg/ml) at room temperature for 10 min was performed to lyse the released Leydig cells. After three washing steps with DMEM/F12, the resuspended cells were subjected to digestion with collagenase/DNase (0.5 mg/ml, 5 µg/ml) two times (5 and 30 min, 35°C) to remove peritubular myoid cells. The last digestion step was applied after three washing steps by adding hyaluronidase/DNase (1 mg/ml, 5 µg/ml) to the cells to break down hyaluronic acid (30 min, 35°C). Washed Sertoli cells were seeded onto Matrigel-coated plates at a density of 0.5×10^6 cells/cm^2 (day 0) and kept in DMEM/F12 supplemented with growth factors (insulin, transferrin, and EGF). After 36 h, remaining sperm cells were removed by hypotonic shock (20 mM Tris, pH 7.4). At day 3 of Sertoli cell culture, germ cells were isolated from adult rat testes by several centrifugation and filtration steps as described by Aravindan et al. (1996). The germ–Sertoli co-culture (cell ratio 5:1) was kept in DMEM/F12 with growth factors plus sodium lactate (6 mM) and sodium pyruvate (2 mM) at 35°C with 5% CO_2. For overexpression of adhesion genes, lentivirus was produced in HEK293T cells by separately cotransfecting (calcium-phosphate method) either human target genes Timp1, Itga5, Tnfrsf12a, Serping1, and Serpina3n (Precision LentiORF or CCSB-Broad lentiviral expression vectors; Thermo Fisher Scientific) or GFP, together with VSV-G packaging (pMD2.G, Addgene) and gag-pol vectors (pCMVΔ8.91, PlasmidFactory). At day 2 of germ–Sertoli co-cultures, either GFP lentivirus alone or a virus mix of five adhesion genes plus an equal amount of GFP virus (as went into controls) was applied to the aliquot wells. At day 5, samples were either harvested for RNA analysis by qRT-PCR or GFP-positive cells were quantified using the Celigo (Cyntellect/Cenibra) and Brooks LifeScience Systems Celigo software. Images were obtained with an inverted microscope (Axiovert 40 CFL) using the Axiovision software (Carl Zeiss).

For in vivo assays, lentiviruses were generated as in the previous paragraph and concentrated by ultracentrifugation. GFP virus or mix + GFP virus was delivered into mouse testes via injection into the efferent ductules by a micropipette as described by Ogawa et al. (1997). Trypan blue (0.02%) was included in the virus suspension to monitor the filling of the seminiferous tubules. Approximately 35 µl of viral suspension (2×10^8 PFU/ml) was injected, filling ~90% of the seminiferous tubules with the viral suspension. 4 and 7 d after injection, mice were sacrificed and the testes were observed under a fluorescence stereomicroscope, followed by processing for H&E to assess the phenotype. Viral expression in testes was verified by GFP IHC staining and qRT-PCR.

Cell culture and cell harvest
The teratocarcinoma GH cell lines and the osteosarcoma Saos-2 cells (parental cells or cell line with inducible TAp73α; Koeppel et al., 2011) were maintained in DMEM supplemented with 10% fetal calf serum at 37°C. In brief, tetracycline-inducible, stable Saos-2 cells were generated by cloning full-length cDNA of TAp73α into the pTRE vector (BD). Afterwards, pTRE-TAp73α vector was cotransfected with the puromycin selection marker containing plasmid pZoneXN into SaOS-2 parental cells using the calcium-phosphate precipitation method. Stable clones were selected with puromycin-containing medium. Expression of TAp73α in stably transfected Saos-2 cells was induced with 0.5 mg doxycycline for 24 h. For transient overexpression, GH cells were seeded to 70% density and transiently transfected with pcDNA3.1-TAp73α or -GFP control for 24 h using the calcium-phosphate method. Saos-2 and GH cells were harvested either for mRNA expression analysis or ChIP analysis, accompanied by Western blot (WB) control staining of the TAp73 overexpression using standard methods. The following antibodies were used: rabbit IgG (2 µg in ChIP, ab46540, rabbit anti–mouse; Abcam), p73 (2 µg in

ChIP and 1:1,000 in WB, ab14430, rabbit anti–human; Abcam), active polymerase II CTD repeat (phosphoS2; 2 µg in ChIP, ab5095, rabbit anti–*Saccharomyces cerevisiae*; Abcam), histone H2B (1:1,000 in WB, 07-371, rabbit anti–human; EMD Millipore), and β-actin (1:5,000 in WB, ab8227-50, rabbit anti–human; Abcam).

qRT-PCR

For mRNA analysis, total RNA was isolated from germ cell pellet, Sertoli cells, transduced germ–Sertoli cocultures, and testis tissue with TRIzol. Reverse transcription was done using M-MuLV reverse transcription (NEB) plus random nonamer/oligo-dT primer mixture. ChIP and cDNA samples were analyzed by SYBR green qRT-PCR. The following ingredients were used for qRT-PCR: 75 mM Tris-HCl, pH 8.8, 20 mM $(NH_4)_2SO_4$, 0.01% Tween 20, 3 mM $MgCl_2$, 0.25% Triton X-100, 300 mM trehalose, 200 mM dNTPs, 1:80,000 SYBR green I (Invitrogen), 0.5 U per reaction Taq DNA polymerase (Primetech), and 600 nM primers. Primer sequences are listed in Tables S3–S6. Gene expression was normalized to 36B4 (murine samples) or HPRT (human cell lines) levels and calculated using the $2^{-\Delta\Delta Ct}$ method. For colorimetric RNA in situ hybridization, a probe set specifically hybridizing to mouse Trp73 (QuantiGene View mRNA; Affymetrix) was used according to the manufacturer's instructions.

Microarrays

To compare mRNA expression from whole testes or specifically germ and Sertoli cells between TAp73KO and WT, whole genome microarrays were performed in the Transcriptome Core Facility, University of Göttingen (GEO dataset accession nos. GSE46034 and GSE52124, respectively). In each case, three 10-wk or 6–8-mo-old mice per genotype were analyzed with the threshold set to twofold difference. Induction/repression was calculated as $\log_2$ values.

ChIP sequencing and ChIP analysis

ChIP sequencing tracks of global TAp73 binding sites were taken from Koeppel et al. (2011; GEO dataset accession no. GSE15780). For ChIP analysis of p73 and active RNA Polymerase II binding sites, chromatin harvest and ChIP analysis was basically done as described by Denissov et al. (2007). In brief, TAp73α-expressing GH or Saos-2 cells were cross-linked with 1% formaldehyde for 30 min. Cross-linking was stopped by adding glycin. After cell lysis, cells were sonicated three times for 10 min using a Bioruptor (Diagenode; high power, 30 s on/off) in the presence of 0.3% SDS. Afterwards, centrifugation removed unsheared chromatin. An aliquot of sheared chromatin was de-cross-linked and served as the input control. For immunoprecipitation, chromatin was incubated with Protein A/G plus Agarose beads (sc-2003; Santa Cruz Biotechnology, Inc.) and 2 µg of p73 (ab14430, rabbit anti–human; Abcam), active polymerase II (ab5095, rabbit anti–*Saccharomyces cerevisiae*; Abcam) or IgG (ab2410, rabbit anti–human; Abcam) antibody overnight, rotating at 4°C. Afterward, ChIP reactions were extensively washed using four different wash buffers, eluted from the beads, and finally de-cross-linked for 4 h at 65°C in the presence of 0.2 M NaCl. After de-cross-linking, the DNA was purified using phenol-chloroform (pH 8.0) and precipitated with ethanol. Ultimately, purified DNA was resuspended in 100 µl of nuclease free water and analyzed by real-time qPCR. Analysis of the myoglobin promoter (myo) by real-time qPCR served as an internal negative control, thereby validating the specificity of the ChIP assay.

Genotyping of p73 and TAp73 mice

For sequence-specific genotyping, genomic DNA was isolated from tail biopsies using the Invisorb Spin Tissue Mini kit (Stratec). PCR was performed by applying standard protocols. Primer sequences are listed in Table S4. PCR products were analyzed by agarose electrophoresis.

Measurement of serum hormone levels

Serum levels of follicle-stimulating hormone (FSH), luteinizing hormone (LH), and testosterone were analyzed by hormone-specific ELISA assays using purified serum obtained from p73KO, TAp73KO, and WT mice. Testosterone levels were measured by Wagnerstibbe using the testosterone II RIA kit (cobas, No. 05200067; Roche). FSH and LH levels were determined by A. Wolfe (Division of Pediatric Endocrinology, Johns Hopkins University, Baltimore, MD) using the bead-based Luminex ELISA assay (EMD Millipore).

Statistical analysis

Statistical calculations were performed with Excel software (Microsoft). Significance was determined using the unpaired one-tailed Student's t test. Significance was assumed for $P < 0.05$. Asterisks indicate: *, $P < 0.05$; **, $P < 0.01$; and ***, $P < 0.005$. ns, not significant.

Online supplemental material

Fig. S1 compares the testicular morphology of ΔNp73, p73KO, and TAp73KO mice. Fig. S2 shows that the hormonal hypothalamic–pituitary–testicular axis remains unaffected in p73KO and TAp73KO mice. Fig. S3 shows the impaired Seroli cell morphology in p73KO and TAp73KO mice. Fig. S4 shows that TAp73 directly regulates the expression of adhesion- and migration-associated genes. Fig. S5 shows that TAp73 does not regulate transcription in Sertoli cells. Table S1 lists adhesion- and migration-associated genes that are deregulated in whole TAp73 testis. Table S2 lists deregulated adhesion- and migration-associated genes in TAp73KO testis and germ cells. Table S3 lists murine primers for qRT-PCR. Table S4 lists the primers for PCR genotyping. Table S5 lists rat primers used for qRT-PCR. Table S6 lists human primers that were used for qRT-PCR and ChIP assays. Table S7 describes the lentiviral constructs used for overexpression of adhesion genes. Online supplemental material is available at http://www.jcb.org/cgi/content/full/jcb.201306066/DC1. Additional data are available in the JCB DataViewer at http://dx.doi.org/10.1083/jcb.201306066.dv.

References

Ahmed, E.A., A.D. Barten-van Rijbroek, H.B. Kal, H. Sadri-Ardekani, S.C. Mizrak, A.M. van Pelt, and D.G. de Rooij. 2009. Proliferative activity in vitro and DNA repair indicate that adult mouse and human Sertoli cells are not terminally differentiated, quiescent cells. *Biol. Reprod.* 80:1084–1091. http://dx.doi.org/10.1095/biolreprod.108.071662

Aravindan, G.R., C.P. Pineau, C.W. Bardin, and C.Y. Cheng. 1996. Ability of trypsin in mimicking germ cell factors that affect Sertoli cell secretory function. *J. Cell. Physiol.* 168:123–133. http://dx.doi.org/10.1002/(SICI)1097-4652(199607)168:1<123::AID-JCP15>3.0.CO;2-8

Aumüller, G., M. Steinbrück, W. Krause, and H.J. Wagner. 1988. Distribution of vimentin-type intermediate filaments in Sertoli cells of the human testis, normal and pathologic. *Anat. Embryol. (Berl.).* 178:129–136. http://dx.doi.org/10.1007/BF02463646

Bartles, J.R., A. Wierda, and L. Zheng. 1996. Identification and characterization of espin, an actin-binding protein localized to the F-actin-rich junctional plaques of Sertoli cell ectoplasmic specializations. *J. Cell Sci.* 109:1229–1239.

Beumer, T.L., H.L. Roepers-Gajadien, I.S. Gademan, P.P. van Buul, G. Gil-Gomez, D.H. Rutgers, and D.G. de Rooij. 1998. The role of the tumor suppressor p53 in spermatogenesis. *Cell Death Differ.* 5:669–677. http://dx.doi.org/10.1038/sj.cdd.4400396

Beyer, U., J. Moll-Rocek, U.M. Moll, and M. Dobbelstein. 2011. Endogenous retrovirus drives hitherto unknown proapoptotic p63 isoforms in the male germ line of humans and great apes. *Proc. Natl. Acad. Sci. USA.* 108:3624–3629. http://dx.doi.org/10.1073/pnas.1016201108

Borg, C.L., K.M. Wolski, G.M. Gibbs, and M.K. O'Bryan. 2010. Phenotyping male infertility in the mouse: how to get the most out of a 'non-performer'. *Hum. Reprod. Update.* 16:205–224. http://dx.doi.org/10.1093/humupd/dmp032

Castrillon, D.H., B.J. Quade, T.Y. Wang, C. Quigley, and C.P. Crum. 2000. The human VASA gene is specifically expressed in the germ cell lineage. *Proc. Natl. Acad. Sci. USA.* 97:9585–9590. http://dx.doi.org/10.1073/pnas.160274797

Charron, Y., R. Madani, S. Nef, C. Combepine, J. Govin, S. Khochbin, and J.D. Vassalli. 2006. Expression of serpinb6 serpins in germ and somatic cells of mouse gonads. *Mol. Reprod. Dev.* 73:9–19. http://dx.doi.org/10.1002/mrd.20385

Cooke, H.J., and P.T. Saunders. 2002. Mouse models of male infertility. *Nat. Rev. Genet.* 3:790–801. http://dx.doi.org/10.1038/nrg911

Coutandin, D., H.D. Ou, F. Löhr, and V. Dötsch. 2010. Tracing the protectors path from the germ line to the genome. *Proc. Natl. Acad. Sci. USA.* 107:15318–15325. http://dx.doi.org/10.1073/pnas.1001069107

Denissov, S., M. van Driel, R. Voit, M. Hekkelman, T. Hulsen, N. Hernandez, I. Grummt, R. Wehrens, and H. Stunnenberg. 2007. Identification of novel functional TBP-binding sites and general factor repertoires. *EMBO J.* 26:944–954. http://dx.doi.org/10.1038/sj.emboj.7601550

Derry, W.B., A.P. Putzke, and J.H. Rothman. 2001. *Caenorhabditis elegans* p53: role in apoptosis, meiosis, and stress resistance. *Science*. 294:591–595. http://dx.doi.org/10.1126/science.1065486

Dötsch, V., F. Bernassola, D. Coutandin, E. Candi, and G. Melino. 2010. p63 and p73, the ancestors of p53. *Cold Spring Harb. Perspect. Biol.* 2:a004887. http://dx.doi.org/10.1101/cshperspect.a004887

Ghafari, F., S. Pelengaris, E. Walters, and G.M. Hartshorne. 2009. Influence of p53 and genetic background on prenatal oogenesis and oocyte attrition in mice. *Hum. Reprod.* 24:1460–1472. http://dx.doi.org/10.1093/humrep/dep022

Griswold, M.D. 1998. The central role of Sertoli cells in spermatogenesis. *Semin. Cell Dev. Biol.* 9:411–416. http://dx.doi.org/10.1006/scdb.1998.0203

Guerquin, M.J., C. Duquenne, H. Coffigny, V. Rouiller-Fabre, R. Lambrot, M. Bakalska, R. Frydman, R. Habert, and G. Livera. 2009. Sex-specific differences in fetal germ cell apoptosis induced by ionizing radiation. *Hum. Reprod.* 24:670–678. http://dx.doi.org/10.1093/humrep/den410

Guyot, R., S. Magre, P. Leduque, and B. Le Magueresse-Battistoni. 2003. Differential expression of tissue inhibitor of metalloproteinases type 1 (TIMP-1) during mouse gonad development. *Dev. Dyn.* 227:357–366. http://dx.doi.org/10.1002/dvdy.10321

Held, T., I. Paprotta, J. Khulan, B. Hemmerlein, L. Binder, S. Wolf, S. Schubert, A. Meinhardt, W. Engel, and I.M. Adham. 2006. Hspa4l-deficient mice display increased incidence of male infertility and hydronephrosis development. *Mol. Cell. Biol.* 26:8099–8108. http://dx.doi.org/10.1128/MCB.01332-06

Holembowski, L., R. Schulz, F. Talos, A. Scheel, S. Wolff, M. Dobbelstein, and U. Moll. 2011. While p73 is essential, p63 is completely dispensable for the development of the central nervous system. *Cell Cycle*. 10:680–689. http://dx.doi.org/10.4161/cc.10.4.14859

Koeppel, M., S.J. van Heeringen, D. Kramer, L. Smeenk, E. Janssen-Megens, M. Hartmann, H.G. Stunnenberg, and M. Lohrum. 2011. Crosstalk between c-Jun and TAp73α/β contributes to the apoptosis-survival balance. *Nucleic Acids Res.* 39:6069–6085. http://dx.doi.org/10.1093/nar/gkr028

Lee, N.P., and C.Y. Cheng. 2004. Ectoplasmic specialization, a testis-specific cell-cell actin-based adherens junction type: is this a potential target for male contraceptive development? *Hum. Reprod. Update*. 10:349–369. http://dx.doi.org/10.1093/humupd/dmh026

Le Magueresse-Battistoni, B. 2007. Serine proteases and serine protease inhibitors in testicular physiology: the plasminogen activation system. *Reproduction*. 134:721–729. http://dx.doi.org/10.1530/REP-07-0114

Le Magueresse-Battistoni, B., G. Pernod, F. Sigillo, L. Kolodié, and M. Benahmed. 1998. Plasminogen activator inhibitor-1 is expressed in cultured rat Sertoli cells. *Biol. Reprod.* 59:591–598. http://dx.doi.org/10.1095/biolreprod59.3.591

Matsui, Y., R. Nagano, and M. Obinata. 2000. Apoptosis of fetal testicular cells is regulated by both p53-dependent and independent mechanisms. *Mol. Reprod. Dev.* 55:399–405. http://dx.doi.org/10.1002/(SICI)1098-2795(200004)55:4<399::AID-MRD7>3.0.CO;2-C

Mruk, D.D., and C.Y. Cheng. 2004. Sertoli-Sertoli and Sertoli-germ cell interactions and their significance in germ cell movement in the seminiferous epithelium during spermatogenesis. *Endocr. Rev.* 25:747–806. http://dx.doi.org/10.1210/er.2003-0022

Mruk, D.D., and C.Y. Cheng. 2011. An in vitro system to study Sertoli cell blood-testis barrier dynamics. *Methods Mol. Biol.* 763:237–252. http://dx.doi.org/10.1007/978-1-61779-191-8_16

Mruk, D., L.J. Zhu, B. Silvestrini, W.M. Lee, and C.Y. Cheng. 1997. Interactions of proteases and protease inhibitors in Sertoli-germ cell cocultures preceding the formation of specialized Sertoli-germ cell junctions in vitro. *J. Androl.* 18:612–622.

Mruk, D.D., M.K. Siu, A.M. Conway, N.P. Lee, A.S. Lau, and C.Y. Cheng. 2003. Role of tissue inhibitor of metalloproteases-1 in junction dynamics in the testis. *J. Androl.* 24:510–523.

Nalam, R.L., C. Andreu-Vieyra, R.E. Braun, H. Akiyama, and M.M. Matzuk. 2009. Retinoblastoma protein plays multiple essential roles in the terminal differentiation of Sertoli cells. *Mol. Endocrinol.* 23:1900–1913. http://dx.doi.org/10.1210/me.2009-0184

Odet, F., A. Verot, and B. Le Magueresse-Battistoni. 2006. The mouse testis is the source of various serine proteases and serine proteinase inhibitors (SERPINs): Serine proteases and SERPINs identified in Leydig cells are under gonadotropin regulation. *Endocrinology*. 147:4374–4383. http://dx.doi.org/10.1210/en.2006-0484

Ogawa, T., J.M. Aréchaga, M.R. Avarbock, and R.L. Brinster. 1997. Transplantation of testis germinal cells into mouse seminiferous tubules. *Int. J. Dev. Biol.* 41:111–122.

Pankow, S., and C. Bamberger. 2007. The p53 tumor suppressor-like protein nvp63 mediates selective germ cell death in the sea anemone *Nematostella vectensis*. *PLoS ONE*. 2:e782. http://dx.doi.org/10.1371/journal.pone.0000782

Petre-Lazar, B., G. Livera, S.G. Moreno, E. Trautmann, C. Duquenne, V. Hanoux, R. Habert, and H. Coffigny. 2007. The role of p63 in germ cell apoptosis in the developing testis. *J. Cell. Physiol.* 210:87–98. http://dx.doi.org/10.1002/jcp.20829

Robinson, L.L., N.A. Sznajder, S.C. Riley, and R.A. Anderson. 2001. Matrix metalloproteinases and tissue inhibitors of metalloproteinases in human fetal testis and ovary. *Mol. Hum. Reprod.* 7:641–648. http://dx.doi.org/10.1093/molehr/7.7.641

Schumacher, B., K. Hofmann, S. Boulton, and A. Gartner. 2001. The *C. elegans* homolog of the p53 tumor suppressor is required for DNA damage-induced apoptosis. *Curr. Biol.* 11:1722–1727. http://dx.doi.org/10.1016/S0960-9822(01)00534-6

Sipione, S., K.C. Simmen, S.J. Lord, B. Motyka, C. Ewen, I. Shostak, G.R. Rayat, J.M. Dufour, G.S. Korbutt, R.V. Rajotte, and R.C. Bleackley. 2006. Identification of a novel human granzyme B inhibitor secreted by cultured sertoli cells. *J. Immunol.* 177:5051–5058.

Siu, M.K., W.M. Lee, and C.Y. Cheng. 2003. The interplay of collagen IV, tumor necrosis factor-α, gelatinase B (matrix metalloprotease-9), and tissue inhibitor of metalloproteases-1 in the basal lamina regulates Sertoli cell-tight junction dynamics in the rat testis. *Endocrinology*. 144:371–387. http://dx.doi.org/10.1210/en.2002-220786

Suh, E.K., A. Yang, A. Kettenbach, C. Bamberger, A.H. Michaelis, Z. Zhu, J.A. Elvin, R.T. Bronson, C.P. Crum, and F. McKeon. 2006. p63 protects the female germ line during meiotic arrest. *Nature*. 444:624–628. http://dx.doi.org/10.1038/nature05337

Talos, F., A. Abraham, A.V. Vaseva, L. Holembowski, S.E. Tsirka, A. Scheel, D. Bode, M. Dobbelstein, W. Brück, and U.M. Moll. 2010. p73 is an essential regulator of neural stem cell maintenance in embryonal and adult CNS neurogenesis. *Cell Death Differ.* 17:1816–1829. http://dx.doi.org/10.1038/cdd.2010.131

Tissir, F., A. Ravni, Y. Achouri, D. Riethmacher, G. Meyer, and A.M. Goffinet. 2009. DeltaNp73 regulates neuronal survival in vivo. *Proc. Natl. Acad. Sci. USA*. 106:16871–16876. http://dx.doi.org/10.1073/pnas.0903191106

Tomasini, R., K. Tsuchihara, M. Wilhelm, M. Fujitani, A. Rufini, C.C. Cheung, F. Khan, A. Itie-Youten, A. Wakeham, M.S. Tsao, et al. 2008. TAp73 knockout shows genomic instability with infertility and tumor suppressor functions. *Genes Dev.* 22:2677–2691. http://dx.doi.org/10.1101/gad.1695308

Xia, W., D.D. Mruk, W.M. Lee, and C.Y. Cheng. 2005. Cytokines and junction restructuring during spermatogenesis—a lesson to learn from the testis. *Cytokine Growth Factor Rev.* 16:469–493. http://dx.doi.org/10.1016/j.cytogfr.2005.05.007

Yan, H.H., D.D. Mruk, W.M. Lee, and C.Y. Cheng. 2007. Ectoplasmic specialization: a friend or a foe of spermatogenesis? *Bioessays*. 29:36–48. http://dx.doi.org/10.1002/bies.20513

Yang, A., R. Schweitzer, D. Sun, M. Kaghad, N. Walker, R.T. Bronson, C. Tabin, A. Sharpe, D. Caput, C. Crum, and F. McKeon. 1999. p63 is essential for regenerative proliferation in limb, craniofacial and epithelial development. *Nature*. 398:714–718. http://dx.doi.org/10.1038/19539

Yang, A., N. Walker, R. Bronson, M. Kaghad, M. Oosterwegel, J. Bonnin, C. Vagner, H. Bonnet, P. Dikkes, A. Sharpe, et al. 2000. p73-deficient mice have neurological, pheromonal and inflammatory defects but lack spontaneous tumours. *Nature*. 404:99–103. http://dx.doi.org/10.1038/35003607